Chapter 1

Photon Detection System

1.1 Introduction

Energy deposition from the passage of high energy charged particles in liquid argon (LAr) yields both free charge from ionization and fast scintillation light. In fact, LAr is an excellent scintillator producing ∼25,000 photons per MeV of energy deposited by a minimum ionizing particle (MIP) in the presence of an electric field (E field) of 500 V/cm. Scintillation light provides information on three key detection aspects of the experiment: event triggering, event (and sub-event) precision time reconstruction, and event energy reconstruction as discussed in Chapter **??**.

The mechanism for light production is quite well understood. Ionized and excited argon atoms combine on a picosecond timescale to produce Ar_2^* singlet or triplet excimer states that rapidly decay (about 25% with a time constant of $\tau_s = 6$ ns, and 75% with $\tau_t = 1.5$ μs) yielding a characteristic scintillation of 128 nm wavelength [**?**, **?**]. In the environment of LAr doped with a small amount of xenon, the slow argon scintillation component is almost entirely shifted to 175 nm [**?**, **?**]. This has the effect of increasing the scattering length for that component to approximately eight times higher than for 128 nm light with the impact that a higher amount of light is collected by the detector for sources beyond ∼4 meters [**?**]. Xenon doping is assumed for the vertical drift detector module (FD2-VD) and this effect is included in all relevant simulations.

The presence of nitrogen impurities in LAr affects both scintillation light production and propagation. Nitrogen affects the light output of argon through non-radiative collisional reactions that destroy the argon excimers before deexcitation, thus quenching scintillation light production. This process particularly affects the long-lived triplet excimer states, effectively reducing the amplitude of the slow component of the argon scintillation light [**?**]. In argon doped with xenon, the vast majority of the argon light that would otherwise be quenched by nitrogen impurities (via $Ar_2^* + N_2 \rightarrow 2Ar + N_2$) can be recovered (via the competing process $Ar_2^* + Xe \rightarrow ArXe^* + Ar$). The impact of nitrogen on scintillation light propagation is that it can absorb VUV photons, reducing argon transparency. Here again, xenon doping helps to mitigate this detrimental effect of nitrogen, since the photoabsorption cross-section by nitrogen is higher at 128 nm than at 175 nm [**?**].

DRAFT

Photon detectors (PDs) are implemented in liquid argon time-projection chamber (LArTPC) experiments to exploit the information provided by scintillation light and thereby both improve and expand the capabilities of the apparatus. The physics motivation for the system capabilities is presented in Section **??**. In the FD2-VD proposal for the second DUNE far detector module, the implementation of a robust PDS is an important feature of the design.

The FD2-VD design will implement the same X-ARAPUCA photon detection system (PDS) technology as the horizontal drift detector module (FD1-HD) design [**?**] but with a modified configuration. Functionally, an X-ARAPUCA module is a light trap that captures wavelength-shifted photons inside boxes with highly reflective internal surfaces until they are eventually detected by silicon photomultipliers (SiPMs). The wavelength-shifted photons are converted to electrical signals by SiPMs distributed evenly around the perimeter of the wavelength-shifting (WLS) plate. Figure 1.1 shows a full-scale X-ARAPUCA PD module prototype.

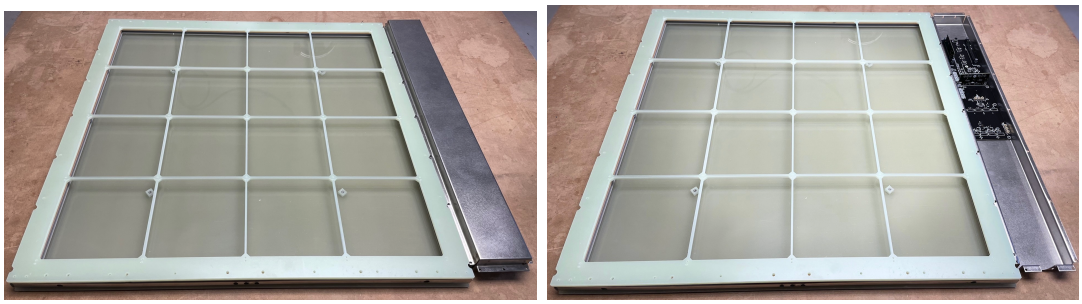

Figure 1.1: Full-scale prototype of the X-ARAPUCAs with (left) and without (right) the electronics cover.

In the vertical drift time projection chamber (TPC) configuration, even though the charge-readout plane (CRP) structure is perforated, it is effectively opaque to light and therefore does not allow for PD installation at the anode (ground) side of the TPC volume. This has the consequence that the PDs can only be installed on the cathode plane, on the field cage walls or on the cryostat membrane walls behind the field cage, provided that the latter is sufficiently transparent to light.

In the FD2-VD PDS design, X-ARAPUCAs are mounted on all four membrane walls (at ground potential) and within the cathode plane structure, as shown in Figures 1.2 and 1.3. Cathode-mount PDs are at the cathode voltage, so there can be no conductive path to ground.

While membrane-mount PDs will adopt the same copper-based sensor biasing and readout techniques as FD1-HD, cathode-mount PDs require new solutions to meet the challenging constraint imposed by operation in a high voltage (HV) environment. The cathode-mount PDs are powered using non-conductive power-over-fiber (PoF) technology [**?**], and the output signals are transmitted through non-conductive optical fibers, i.e., signal-over-fiber (SoF) technology. This solution provides voltage isolation in both signal reception and transmission. PoF is a well established technology, but its extensive use in a cryogenic detector will be a new application.

Another important difference of the FD2-VD design with respect to FD1-HD, which has smaller optical volumes, is the doping of LAr with xenon at the level of $\mathcal{O}(10\,\mathrm{ppm})$[1]. Results from large-

[1] Although the baseline FD1-HD design does not call for xenon doping, the cryogenics system allows the option for addition of a xenon injection port as a potential mitigation for nitrogen contamination.

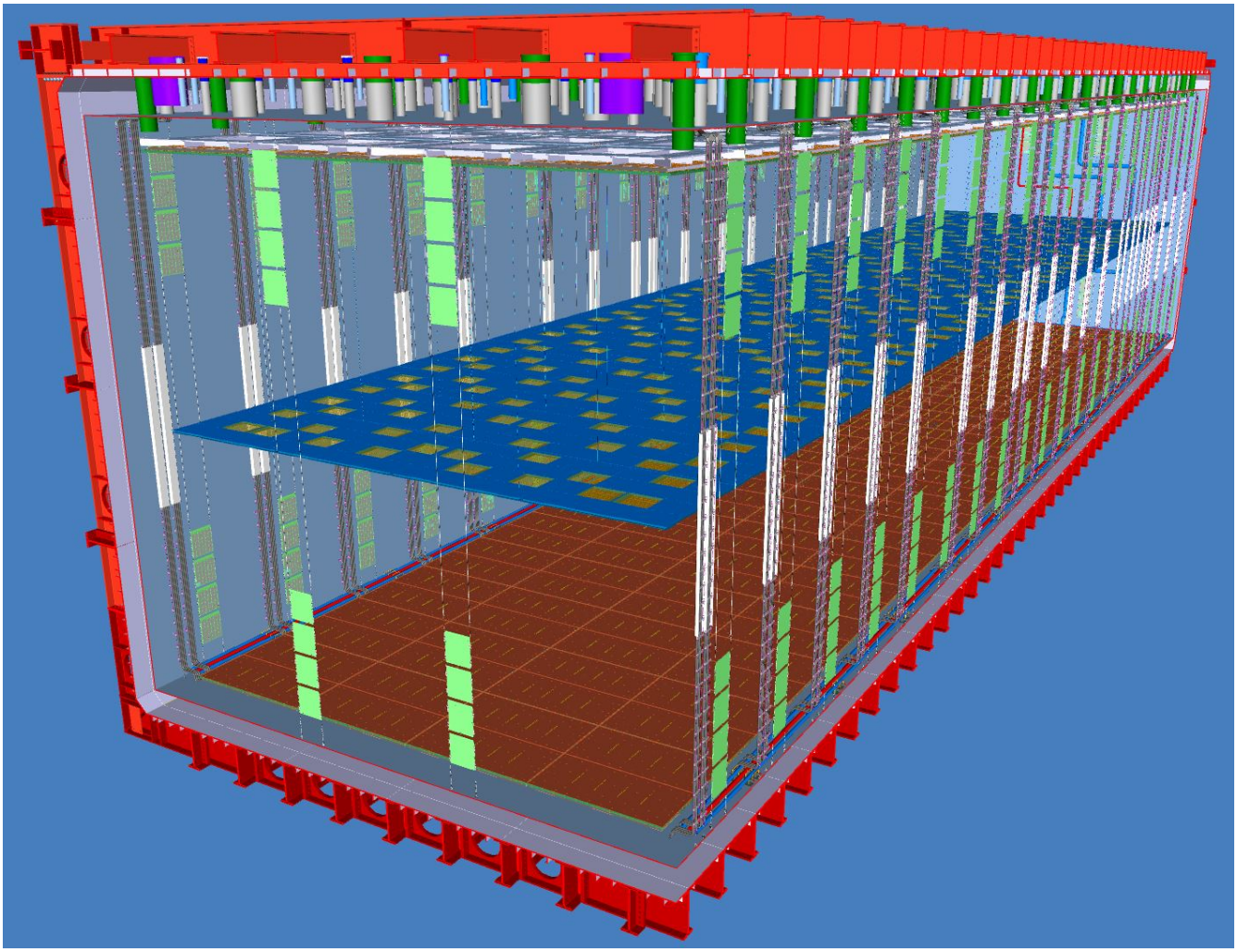

Figure 1.2: Perspective view of X-ARAPUCA modules locations on the horizontal cathode plane and on the vertical cryostat membrane walls behind the field cage.

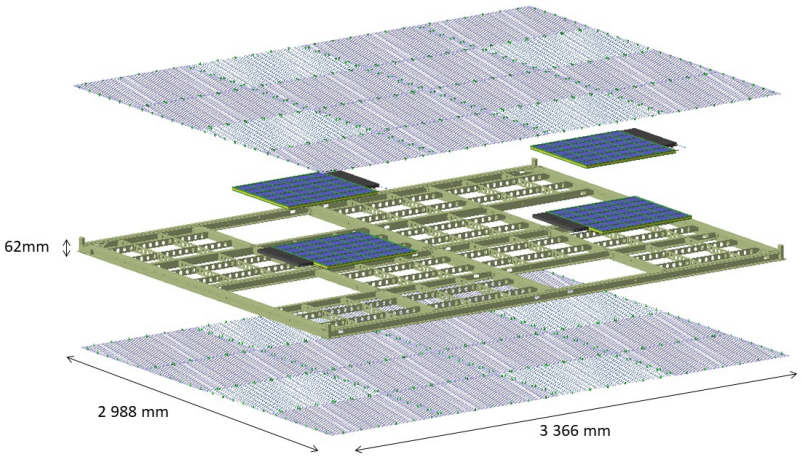

Figure 1.3: A cathode plane module showing the placement of the four FD2-VD PDS X-ARAPUCAs in the central modules (blue squares). In the cathode plane modules adjacent to the field cage, there are no PD modules abutting the field cage to minimize potential discharge effects. The cathode module has a resistive skin over most of the surface, except for a conductive mesh of 90% optical transparency over the X-ARAPUCAs.

volume measurements with ProtoDUNE-SP and ProtoDUNE-DP are summarized in Section 1.8.1. This feature will ensure improved light detection uniformity (see Figure 1.4) and will make the system more resilient to nitrogen contamination. In particular, the ratio of minimum-to-average light yield (LY) in the z=0 plane of the active volume improves from 0.16 for pure argon to 0.51 for Xe-doped argon.

As shown in Section 1.2.1, the FD2-VD PDS configuration, with uniformly distributed PD coverage across the cathode and partial coverage on all four membrane walls near the anode planes, produces significantly better overall light yield and light yield uniformity across the entire TPC active volume when compared to the FD1-HD design for a comparable cost.

1.2 Design Specifications, Performance and Scope

1.2.1 Specifications and Performance

The detector specifications for the FD2-VD PDS are the same as for the FD1-HD system. Selected specifications, those with a direct connection with physics performance, are reproduced here in Table 1.1. The proposed system will exceed these requirements, as summarized in Table 1.2 and described below, providing a robust margin against unexpected degradation and may enhance the system performance for some physics studies.

The light yield (LY, detected photons per unit deposited energy) is the most important PDS specification in Table 1.1 (first row). Both the average LY from light emission anywhere in the detector volume, and the lowest detectable light level from the dimmest part of the detector, are relevant. For PDs located on a single detection surface, the LY variation across the volume would present a large gradient along a perpendicular axis to this plane. Placing photosensors along the

Table 1.1: Key FD2-VD PDS specifications.

No.	Description	Specification	Rationale
1	Light yield	>20 PE/MeV (avg), >0.5 PE/MeV (min)	Gives PDS energy resolution comparable to that of the TPC for 5-7 MeV supernova (SN) ν's, and allows tagging of > 99% of nucleon decay backgrounds with light at all points in detector.
2	Time resolution	$< 1\,\mu$s Goal: < 100 ns	Enables 1 mm position resolution along drift direction.
3	Spatial localization in plane perpendicular to drift	< 2.5 m	Enables accurate matching of PD and TPC signals.
4	Single PE pulse height divided by baseline noise RMS	> 4	Signal-to-noise sufficiently high to keep data rate within electronics bandwidth limits and to ensure efficient trigger.
5	Dark rate per electronics channel	< 1 kHz	Dark noise sufficiently low to keep data rate within electronics bandwidth limits and to ensure efficient trigger.
6	Fraction of beam events with saturating channels	$< 20\%$	Sufficient dynamic range is needed to reconstruct the energy calorimetrically, but a small amount of saturation can be mitigated.

Table 1.2: FD2-VD PDS estimated performance and basis for estimates (see text for details).

No.	Description	Estimated Performance	Basis for Estimate
1	Light yield	$\simeq$39 PE/MeV (avg), $\simeq$16 PE/MeV (min)	Geant4-only simulations.
2	Time resolution	$\simeq$4 ns	ProtoDUNE-SP cosmic-ray data.
3	Spatial localization in plane perpendicular to drift	$\simeq$0.75 m at 400 MeV	Liquid Argon Software (LArSoft) simulations of nucleon decay events.
4	Single PE pulse height divided by baseline noise RMS	6	Cold box tests at CERN and ganging tests in standalone facilities.
5	Dark rate (DCR) per electronics channel	$\simeq$0.2 kHz	Standalone tests at 77 K for 80 ganged SiPMs (verified for both vendors).
6	Fraction of beam events with saturating channels	2% of beam events with > 5% saturated channels	LArSoft simulations of beam neutrino interactions.

four membrane walls in addition to the cathode, as in this system design, significantly reduces the LY non-uniformity along the drift (y) direction.

A dedicated study using a Geant4-only simulation has been performed to determine the LY map of the reference PDS design. Compared to the CDR LY studies that also relied on a Geant4-only simulation, several simulation assumptions affecting the detector geometry, the light production in LAr and the reflectivity of detector materials have been updated. The result is a realistic simulation, based on essentially the same optical assumptions included in the end-to-end LArSoft event processing chain discussed in Section **??**. The advantage of the standalone Geant4 simulation over the LArSoft simulation framework is a much faster turnaround for LY studies for different PDS layout geometries or optical simulation assumptions.

In the Geant4-only simulation used to estimate the LY, the full FD2 geometry is simulated, including the most relevant detector components from the PDS point of view. In particular, the geometry of the thin (∼70% transparent) and thick (optically opaque) field cage profiles, as well as the location of all cathode-mount and membrane-mount X-ARAPUCAs, is accounted for. The average light transmission of the conductive mesh that covers the cathode-mounted module windows is taken to be 90%.

For scintillation light production in LAr, we use 12,700 photons/MeV at 175 nm, plus 7,300 photons/MeV at 128 nm, as inferred from ProtoDUNE-DP Xe-doping data (at 10 ppm Xe). For light propagation in LAr, an absorption length of 80 m (20 m) and a Rayleigh scattering length of 8.5 m (1 m) are assumed at 175 nm (128 nm). This absorption length corresponds to a level of N_2 impurities in the LAr of about 3 ppm, see [**?**]. The reflectivity at 175 nm and 128 nm of the anode PCB, the field cage profiles, and the membrane cryostat wall materials are accounted for in the simulation. Finally, motivated by prototype measurements and simulations [**?**, **?**, **?**, **?**], the X-ARAPUCA detection efficiency is set to the target value of 3% at both 175 nm and 128 nm. In the light yield plots (Figure 1.4) the detection efficiency is a scale factor, as discussed below.

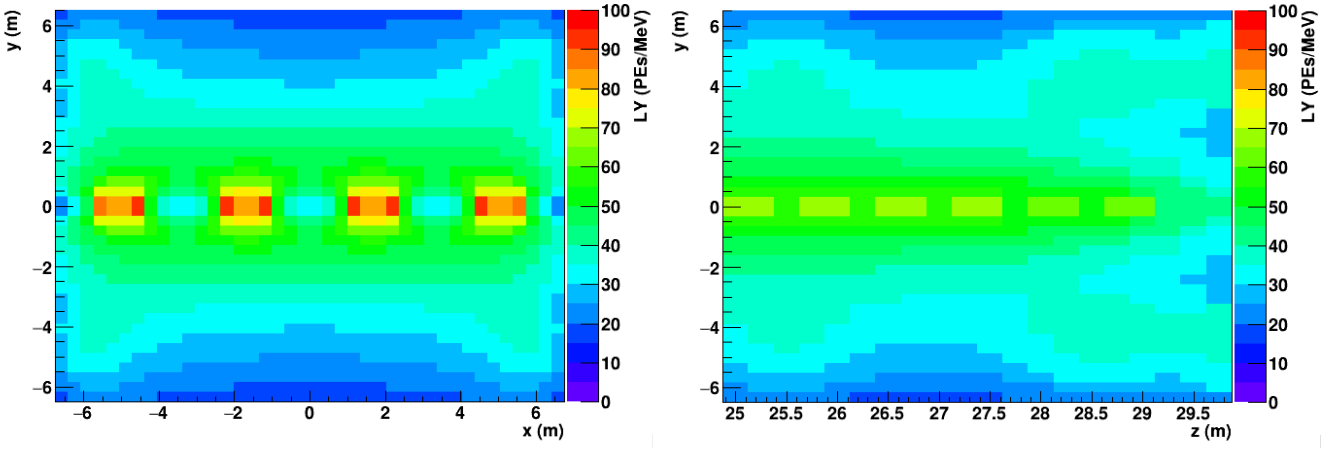

Figure 1.4: (Left) Map of the light yield (LY) in the central (x, y) transverse plane at $z = 0$ for the reference configuration. (Right) Map of LY in the central (z, y) longitudinal plane at $x = 0$, close to the detector boundary at $z = 30$ m in front of one of the membrane short walls, for the same PDS configuration.

The light yield LY(x, y) for the central transverse plane at $z = 0$ inside the target volume was

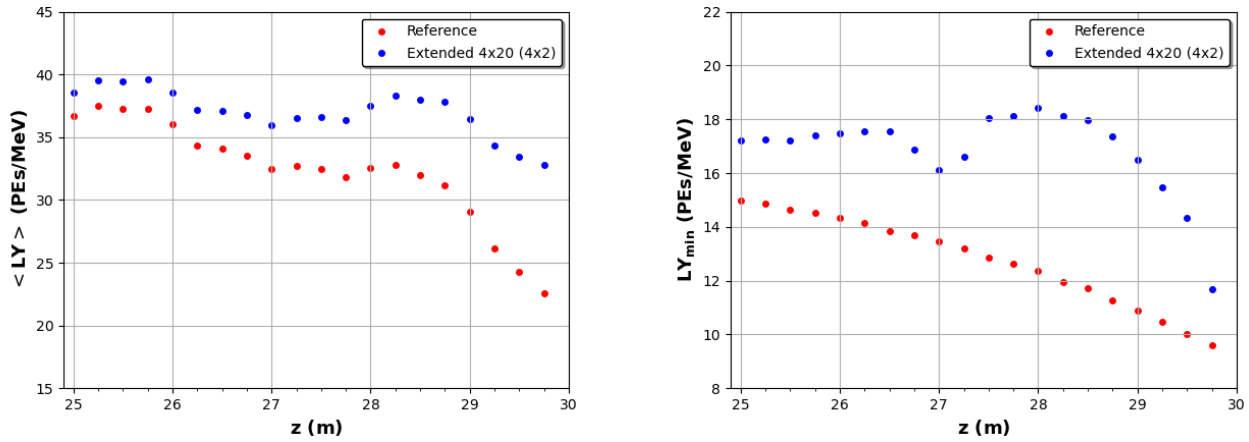

Figure 1.5: Values for average (left) and minimum (right) LY in (x, y) planes as a function of the z direction, obtained close to the detector boundary at $z = 30$ m. Light yield values for two detector configurations are shown: reference configuration including X-ARAPUCAs on the membrane short walls in blue, without short wall X-ARAPUCAs in red.

evaluated and is shown in Figure 1.4 (left).[2] The (z, y) projection of LY for $x = 0$ and near the detector end-wall at $z = 30$ m is shown in Figure 1.4 (right). As is evident in both projections, the LY is highest near the cathode plane at $y = 0$, and lowest near the non-instrumented anode planes at $y = \pm 6.5$ m. The average LY value for events in the $0 < z < 3$ m detector portion near the central transverse plane at $z = 0$ is $\langle \text{LY} \rangle \simeq 39$ PE/MeV, as reported in Table 1.2. Boundary conditions close to either ends of the detector volume at $z = \pm 30$ m also affect the LY.

As shown by the red data points in Figure 1.5, a clear decrease for both average (left) and minimum (right panel) LY per z slice would be observed along the z direction at both detector ends if no X-ARAPUCAs were installed on the membrane short walls. The presence of 32 X-ARAPUCAs in the reference design on the end walls ensures a more uniform LY response along z near the detector boundaries, as shown by the blue points in Figure 1.5. The goal of this modest (5%) coverage increase, compared to the option with non-instrumented end walls, is to enlarge the FD2 fiducial volume for analyses relying on PDS information.

These values significantly exceed the LY specifications of Table 1.1. They are also much better than the FD1-HD PDS values, particularly with regard to the spatial uniformity of the detector response. While these simulation results assume our target X-ARAPUCA detection efficiency of 3%, light yield estimates for the FD2-VD PDS scale linearly with efficiency. Light yield specifications would thus be met even under the worst-case X-ARAPUCA detection efficiency that would satisfy requirements, that is 2% (see Sec. 1.4). As discussed in Table 1.1 and in Section **??**, this high and uniform light yield will ensure a PDS energy resolution comparable to that of the TPC at supernova neutrino burst (SNB) energies, SNB event triggering using PDS information alone, and efficient tagging of nucleon decay backgrounds anywhere in the LAr active volume.

[2]We use the FD2-VD coordinate system: z is parallel to the Far Detector Module's long dimension, aligned with the incident neutrino beam; y is the vertical drift direction; and x is along the module's narrow horizontal dimension. The origin is at the geometric center of the module.

Preliminary time resolution results for an X-ARAPUCA-based PDS have been obtained using the 12 X-ARAPUCA channels in APA6 of ProtoDUNE-SP at CERN. Photons coming from the same cosmic-ray muon track are detected by two separate (nearby) channels. TPC crossing cosmic-ray muon tracks nearly parallel to APA6 are used, such that differences in photon arrival time to the two nearby channels become negligible. To reduce the effect of the 6.67 ns sampling time, the waveforms' rising edges are fitted to extract the time at which the amplitude crosses one photoelectron (PE) for each channel. The difference in time measured by the two channels provides a direct estimate of the single-channel time resolution, measured to be about 4 ns. The time resolution of the optical flashes, being a collection of time-coincident and space-correlated optical hits, is better than 4 ns. Even though this result was obtained with ProtoDUNE-SP data, the similar PDS technology and sampling time ensure that a similar time resolution is expected in FD2-VD, exceeding the time resolution requirement by a large margin.

Initial results on spatial resolution in the FD2-VD and in the plane perpendicular to the drift direction were obtained with a Geant4-only simulation of point-like energy deposits at SNB energies (tens of MeV) and a pseudo-reconstruction relying on the barycenter of the light pattern, see [**?**]. A spatial resolution in the transverse plane of about 0.5 m was obtained. These results have now been confirmed with full LArSoft simulations of nucleon decay events.

For this study, the simulation and reconstruction of 10^5 events has been carried out. The events include GENIE-generated $p \to K^+\bar{\nu}$ decays, one decay per simulated event, uniformly distributed in the LAr volume and depositing about 400 MeV of energy on average. They also model the detector activity due to radiological backgrounds, according to the model in Table **??**. The radiological model introduces a rate of reconstructed optical flashes of about 200 kHz, or about 800 flashes throughout the 4 ms long event time window. For the position reconstruction study, we define the signal-like flash in each event as the flash of highest charge among those with a timing consistent (within ± 1 μs) with the nucleon decay time.

As in our earlier study, the reconstructed position of the nucleon decay candidate event in the plane perpendicular to drift is reconstructed using a simple barycenter algorithm, using position and detected charge information from PDs located on the cathode. The reconstructed position is then compared to the true position of the MC simulated nucleon decay vertex. A spatial resolution of about 75 cm is obtained. This expected performance is significantly better than the 2.5 m spatial resolution required.

The single-photoelectron pulse height divided by the baseline noise root mean square (RMS) (or signal-to-noise (S/N) ratio, in the following[3]) and the dark rate per electronics channel (rows 4 and 5 in Table 1.1), have been studied with ProtoDUNE-SP PDS data, with CERN cold box data, and with dedicated setups. Since the initial cold box runs in August 2022, light leakage from PoF receivers and fibers have been reduced to negligible levels. The S/N ratio measured in a cold box run in February 2023 for a PD module with PoF and SoF readout was 5.9, as shown in Figure 1.29, significantly higher than the specification of 4.

The dark count rate at 77 K of the SiPMs under consideration for FD2-VD (see Section 1.5) has

[3]The S/N ratios quoted throughout the chapter refer to the smallest possible signal of interest for one PD channel, which is a single-photoelectron pulse. Most physics event categories in DUNE will typically produce much larger signals.

been measured to be about 60 mHz/mm^2, corresponding to about 0.2 kHz per electronics channel, which is well within requirements.

Table 1.1 specification No. 6, the maximum fraction of beam events with saturating channels that impacts energy resolution, has been demonstrated in full LArSoft simulations of beam electron neutrino interactions and assuming a 14-bit dynamic range, see Section **??**. It was found that only a 2% (0.2%) of events have more than 5% (10%) PDS channels overflowing the ADC range. Also, this dynamic range induces a mean reduction in the determination of the total deposited energy per event, estimated from the reconstructed charge sum over all optical hits, of only 2%. In other words, PDS channel saturation level in FD2-VD is expected to be within requirements. It is also lower compared to the saturation studies presented in the FD1-HD TDR [**?**], which assumed a 12-bit digitizer.

1.2.2 PD Consortium Scope

The DUNE PD Consortium (see Section 1.14) will provide a photon detector system for FD2-VD that meets the performance requirements established by the DUNE collaboration as presented in Table 1.1. The scope of the consortium activity includes selecting and procuring material for, and the fabrication, testing, delivery and installation of light collectors (X-ARAPUCA), photosensors (SiPMs), electronics, and a calibration and monitoring system. The reference design components are listed in Table 1.3.

Table 1.3: PDS reference configuration

Component	Description	Quantity
Light collector	X-ARAPUCA	352 single-sided modules (160 per long-dimension wall, 16 per short-dimension wall), 320 double-sided modules (cathode plane); 672 total. Light collection area 3600 cm^2/module/side
Photosensor	Hamamatsu and FBK 6 mm SiPM×6 mm	160 SiPMs per module; 107 520 total
SiPM signal summing	5 groups (in series) of 4 SiPMs (in parallel) per flex PCB	8 flex PCBs per module; 5376 total
Readout electronics	Analog signal conditioning circuit	2 channels/module; 1344 total
Calibration and monitoring	Pulsed UV via field cage-mounted fibers	15 fibers per roof penetration; 20 penetrations per side; 600 total

Although the configuration of the FD2-VD and FD1-HD led to structurally different solutions for the PDS, many of scientific and technical issues are similar. A common consortium facilitates the sharing of information and helps to exploit the similarity of these two detectors, as appropriate.

1.3 Photon Detector System Overview

Scintillation light detection in the FD2-VD module is based on the X-ARAPUCA technology developed for the FD1-HD module, with the photocollector design modified to match the different FD2-VD mechanical and electrical constraints. The PDS consists of a large number of photon detection units distributed on or behind the surfaces delimiting the LArTPC active volume. The basic unit is the X-ARAPUCA detector module with a light collecting area of approximately $600 \times 600\,\mathrm{mm}^2$. The modules have light collection windows on either one (single-sided) or two (double-sided) faces, depending on the location in the active volume. The wavelength-shifted photons are converted to an electrical signal by 160 SiPMs distributed evenly around the perimeter of the module. Groups of SiPMs are electrically connected to form just two output signals, each corresponding to the sum of the response of 80 SiPMs.

The FD2-VD PDS topology consists of 320 double-sided X-ARAPUCA modules evenly distributed across the cathode plane (cathode-mount modules) and 352 single-sided modules mounted behind the field cage onto the cryostat walls (membrane-mount modules), as illustrated in Figure 1.2. The 352 membrane-mount modules includes 32 modules on the cryostat end-walls[4].

The cathode-mount X-ARAPUCAs are embedded in the mechanical frames of the central cathode plane, as illustrated in Figure 1.3. They will have two optical surfaces, one facing upward into the top FD2-VD volume, the other facing downward into the bottom volume. Operating photodetectors on a HV surface requires electrically floating photosensors and readout electronics, i.e., power (in) and signal (out) transmitted via non-conductive cables. This is achieved with the use of PoF technology and optical transceivers for communication via SoF technology.

Membrane-mounted X-ARAPUCAs will be arrayed in columns along all four walls of the cryostat. They will face inward from behind the field cage, spanning the vertical ranges $3.3 < y < 6.3\,\mathrm{m}$ and $-6.3 < y < -3.3\,\mathrm{m}$ as measured from the cathode plane, respectively, where the field cage is approximately 70% transparent (Section **??**). They will be supported on hanging vertical mechanical structures, each holding four modules mounted near the top anode plane and four near the bottom. There will be 20 columns on each of the long walls and two columns on each short wall. The column structures are electrically referenced to detector ground and thus do not require PoF and optical transceivers; standard transmission through copper cables will be used for both power and signal, leveraging the FD1-HD experience.

A conceptual diagram of the the SoF and PoF routing for the cathode-mount modules and the copper-based routing for the membrane-mount modules is shown in Figure 1.6.

To optimize the light collection uniformity, the LAr is doped with $\mathcal{O}(10\,\mathrm{ppm})$ xenon, which like argon, is a high-yield scintillator. Several studies have demonstrated its beneficial light production properties when used as a low concentration dopant [**?**, **?**, **?**, **?**]. Motivated by these studies done on smaller LAr volumes, DUNE tested xenon doping in the ProtoDUNE detectors, and concluded that it will provide greater light yield uniformity and allow photon detection recovery from accidental nitrogen contamination for multi-meter drift-path TPCs (see Section 1.8.1).

[4]These were not part of the Conceptual Design Report design, but were added to provide better light-yield uniformity throughout the active volume.

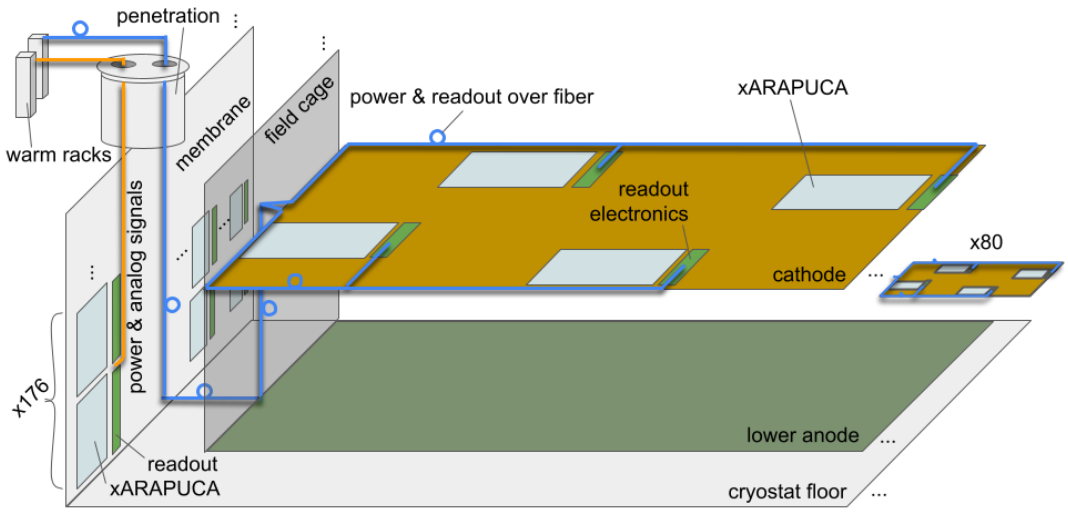

Figure 1.6: Conceptual diagram of power and signal routing. One of the 80 cathode four-module groups (see Figure 1.3) is shown on a greatly expanded scale; fibers pass through holes in the cathode modules, down along the field cage and over to the membrane wall, en route to penetrations on the top surface of the cryostat. More detailed drawings are provided in Section 1.6.2.3.

A concentration of $\mathcal{O}(10\,\text{ppm})$ is sufficient for the Ar triplet scintillation component to be fully transferred to the xenon emission wavelength (175 nm), which reduces the Rayleigh scattering rate of the wavelength-shifted light and so increases collection efficiency for light emitted at a far distance from the PDs. It also mitigates the risk due to inadvertent nitrogen contamination of the LAr. The time response of the PD modules to scintillation light will be used to monitor the xenon content in LAr. ProtoDUNE-SP data have demonstrated that the shape of the average PD modules' waveforms is very sensitive to the xenon concentration.

The basic properties of the scintillation medium, photon collectors, photon sensors and associated electronics for the FD2-VD PDS are summarized in Table 1.4.

The FD2-VD PDS design of 320 cathode mounted X-ARAPUCAs provides 105.6 m^2 photodetector coverage out of the 810 m^2 cathode area, for 13.0% optical coverage. The assemblage of 320 X-ARAPUCAs mounted on the long walls of the cryostat membrane gives 105.6 m^2 coverage which is about 6.8% of the field cage area. Finally, the optical coverage on the cryostat membrane short walls is 10.6 m^2 out of 351 m^2 for 3.0%. Figure 1.7 (left) is a 3D rendering of the FD2-VD showing the top two rows of PDs X-ARAPUCAs (blue) on one long wall and those in the cathode frame. The view is from the opposite cryostat wall, behind the field cage, in the top drift volume.

The field cage electrodes in the foreground are ∼70% transparent to light, allowing transmission to the PD detector modules behind it. This configuration provides the FD2-VD PDS with a photon detection performance that meets the experiment's requirements, as presented in Chapter **??** and Sec. 1.2.

Table 1.4: Summary of FD2-VD PDS scintillation medium and reference design technology.

Item	Description
Liquid argon Scintillator	Ar+Xe (10 ppm). Residual impurity: $[N_2]< 1$ ppm, $[O_2]< 50$ ppt. Absorption length: $\lambda_{abs} \geq 30$ m. Photon yield (MIP, nominal E field =500 V/cm): 25,000 ph/MeV. (Ar-Xe) Energy transfer reaction: Ar triplet scintillation component fully transferred to Xe $\Rightarrow Y_{ph}(\mathrm{Ar}) \simeq 6,000$ ph/MeV, $Y_{ph}(\mathrm{Xe}) \simeq 19,000$ ph/MeV. Rayleigh scattering length: $\lambda_R(\mathrm{Ar}) \simeq 1$m, $\lambda_R(\mathrm{Xe}) \simeq 8.5$m.
Photon collector	X-ARAPUCA (light trapping by dichroic filters and two-stage WLS). Sensitive to both Ar light (128 nm) and Xe light (147 and 175 nm). Detection efficiency $\epsilon_D \simeq 3\%$ (detected PEs per photon impinging upon the optical surface of the detector).
Photosensor	SiPM 6×6 mm^2 area, single-photon sensitive. Requirements at nominal voltage: PDE(450 nm)>35%, dark count rate <200 mHz/mm^2, cross-talk <35%, afterpulse < 5%, gain $> 2 \times 10^6$. Cold electronics (CE) read-out (active ganging, shape and noise filtering). S/N≥ 4

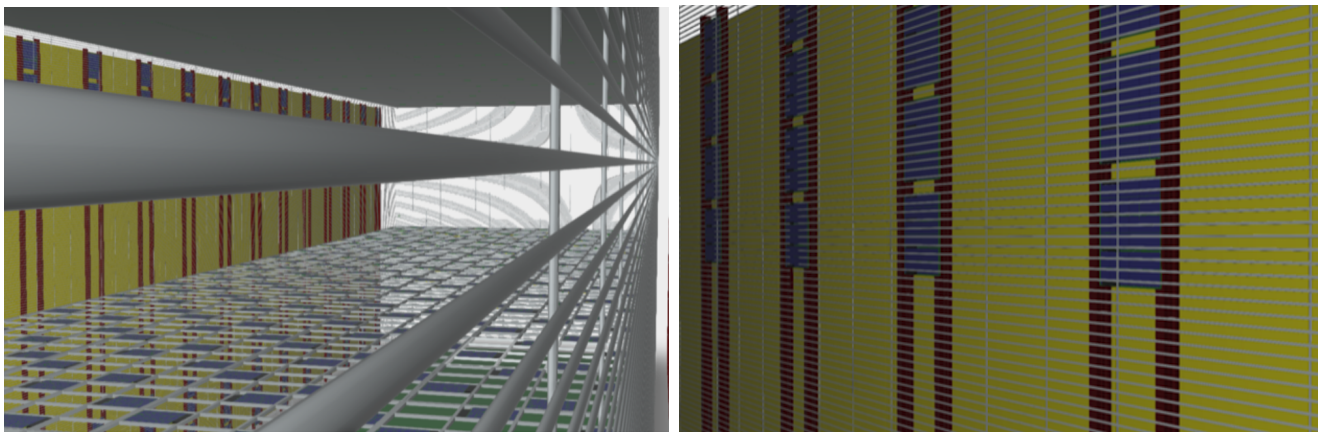

Figure 1.7: X-ARAPUCA detector modules (indigo) on the cathode plane and on the field cage walls – view through ∼70% transparent field cage into detector volume (left); view of the membrane-mount X-ARAPUCA detector modules from inside the active volume (in this close-up view, the field cage bars are visible in front of the modules) (right).

Table 1.5: FD2-VD PDS components.

Item	Quantity	Detector surface
X-ARAPUCA modules	320 double-sided	Cathode plane
	320 single-sided	Membrane long walls
	32 single-sided	Membrane short walls
Dichroic filters	17,856	
WLS plates	672	
Photosensors (SiPMs)	51,200	Cathode plane
	51,200	Membrane long walls
	5,120	Membrane short walls
Signal channels	640	Cathode plane
	640	Membrane long walls
	64	Membrane short walls
SiPMs per channel	80	
Optical Area	$105.6\,\mathrm{m}^2 \times 2$	Cathode plane
	$105.6\,\mathrm{m}^2$	Membrane long walls
	$11.5\,\mathrm{m}^2$	Membrane short walls
Active coverage	13.0%	Cathode plane
	6.8%	Membrane long walls
	3.0%	Membrane short walls

1.4 Light Collectors

The X-ARAPUCA developed for the FD1-HD has been adopted for use in FD2-VD. It offers compact and flexible design geometry and has a very small impact on the LArTPC active volume. The X-ARAPUCA module has an excellent ratio of optical to inactive surface areas (68 %), a good PDE, a moderate fabrication cost, and is relatively easy to integrate into the TPC layout. Table 1.5 itemizes the components of the PDS.

The basic unit of the PDS is a module as depicted in Figure 1.8 with dimensions provided in Table 1.6.

It is a tile-shaped thin module with overall dimensions 653 mm × 653 mm × 29.9 mm plus an attached electronics box 645 mm × 89.6 mm × 42.4 mm, bringing the total outside dimensions to 742.6 mm × 653 mm × 42.4 mm. PD modules are composed of three basic design elements:

- one (single-sided) or two (double-sided) dichroic window frame assemblies composed of 16 PTP-coated dichroic filters mounted in G-10 frames – the dichroic window dimension establishes the active area of the module as 575 mm × 575 mm, $0.33\,\mathrm{m}^2$;
- one frame and Faraday cage shielding assembly consisting of a WLS-doped acrylic plate onto which the SiPMs are coupled (a three-sided conducting box protects the SiPMs from induced currents due to a potential cathode HV discharge, see Section 1.4.1); and
- one cold electronics/PoF/SoF electronics enclosure, mounted to one side of the basic module following assembly.

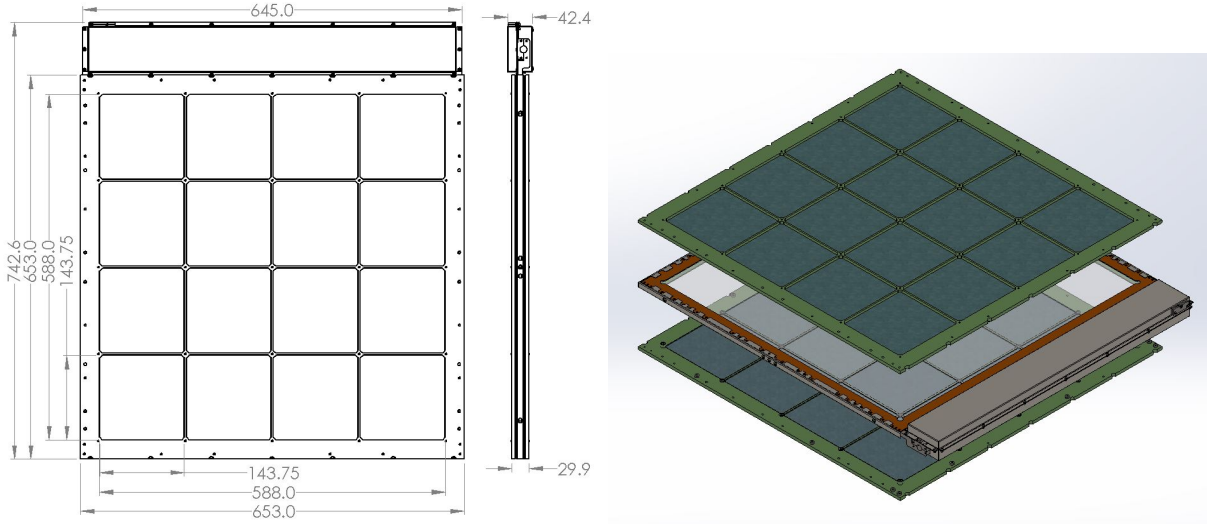

Figure 1.8: (Left) Dimensioned drawing of a FD2-VD PDS detector module. (Right) Exploded view showing major design elements. The double-sided module concept to be used in the cathode is shown (with dichroic filter windows on both sides of the module). For the membrane mount modules, the windows on the side facing the cryostat wall are replaced with a reflector-coated G-10 sheet. [A photograph of a module that will be tested in the cold box at CERN is shown in Figure 1.1.]

Table 1.6: PD basic unit: X-ARAPUCA module.

Item/Parameter	Quantity	Dimensions
Light collection module area (excluding electronics box)	1	$653\,\text{mm} \times 653\,\text{mm} = 0.43\,\text{m}^2$
Module thickness	1	29.9 mm
Weight	1	~ 8.6 kg
Active Area	2 (two-sided)	$0.33\,\text{m}^2$ per side
Dichroic filters	16 × 2 sides	$143.8\,\text{mm} \times 143.8\,\text{mm}$
WLS plate	1	$607\,\text{mm} \times 607\,\text{mm} \times 3.8\,\text{mm}$
SiPMs	160	$6\,\text{mm} \times 6\,\text{mm}$
Read-out channels	2	
SiPMs per channel	80	

The square modular geometry optimizes the ratio of the light collecting area to the SiPM area and the module mechanical design allows use of the same structure for both the cathode-mount and membrane-mount configurations. In the case of the single-sided membrane-mount modules, the rear side (facing the cryostat wall) window frame assembly is removed and replaced by a single sheet of G-10 coated with 3M Vikuiti^{TM} reflective material.

The WLS plate acts as a secondary shifter, serving three main functions: providing the wavelength shift required to trap the photons within the X-ARAPUCA volume, matching the SiPMs wavelength sensitivity, and as a light guide – the optical-grade surfaces enable efficient uniform light collection over a large area. Prototype WLS plate have been manufactured at a casting reactor at UniMIB, while for the large scale production, the Glass to Power s.p.a. company (G2P)[5] G2P has been identified as an industrial partner.

A spring-loaded SiPM mounting system (see Figure 1.9) makes a dynamic connection between the WLS plate and the G-10 frame to allow for relative thermal contraction of the WLS plate and frame.

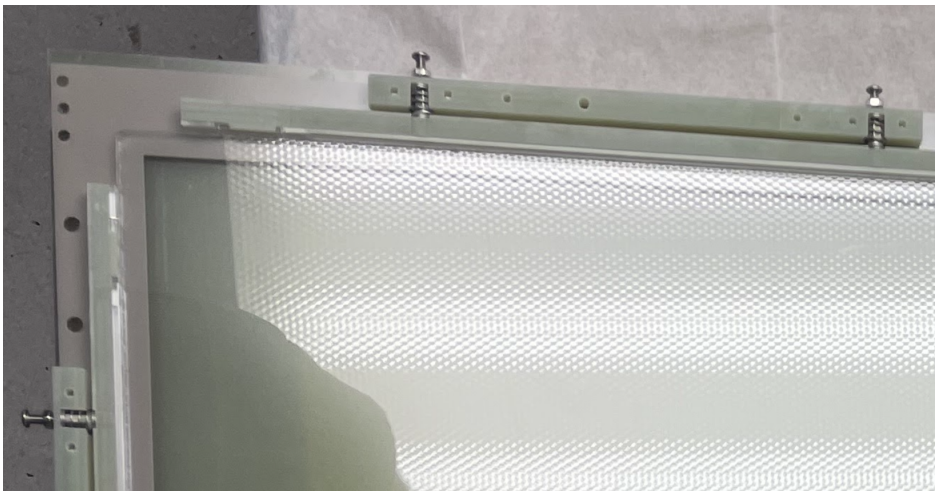

Figure 1.9: WLS plate centered in G-10 frame, held by spring-loaded dynamic mounting system. Coil springs (16 total, three visible in this image) maintain physical contact between the WLS plate and the SiPM face throughout cool-down. Screws (seen in this figure) passing through the springs are used to allow controlled application of force while the SiPMs are installed, then removed following installation.

The SiPMs have dimensions $6\times6\,\mathrm{mm}^2$ and are mounted in a series of five adjacent units of four SiPMs, each passively ganged on one flexible Kapton PCB strip (i.e., one 30 cm flex circuit has 20 SiPMs; see Figure 1.10, left). The SiPMs are positioned symmetrically with respect to the mid-plane of the plate[6].

Each flex circuit mates through a connector to a shielded twisted-pair cable 130 cm long that passively routes the flex circuit signal to the module interface board where a stage of signal shaping

[5]Glass-to-Power - Italy `https://www.glasstopower.com`.

[6]Simulation of two additional SiPM geometries with the same active area ($4\times9\,\mathrm{mm}^2$ and $3\times12\,\mathrm{mm}^2$) in the FD1-HD PD module bar configuration showed no substantial difference in the detection efficiency that would justify a custom geometry for the SiPM.

and buffering prepares the signal for readout. There are eight such flex circuits along the perimeter of the WLS plate, for a total of 160 SiPMs. The SiPMs are grouped into two readout channels of 80 SiPMs each; two channels offer a level of redundancy for the module.

The strips of SiPMs are held against the WLS plate edges by an array of low-strength coil springs. The use of a spring-loaded backing plate and flexible PCBs for mounting (Figure 1.10) the SiPMs combined with dynamic supports for the WLS plate inside the G-10 provides accommodation for the roughly 1% relative thermal contraction between the WLS plate and the G-10 frame during cool-down. A Vikuiti reflector adhered to the Kapton flexi PCB covers the plate edge between adjacent SiPMs.

A possible enhancement of the reference PD module design to enhance the efficiency of photon extraction from the WLS plates onto the SiPMs would be to include cutouts in the WLS plates at the location of the SiPMs. The performance and cost-effectiveness of three different cutout shapes and associated production costs are being evaluated as part of the final module evaluation, with a final decision as to their inclusion decided prior to the production readiness review (PRR).

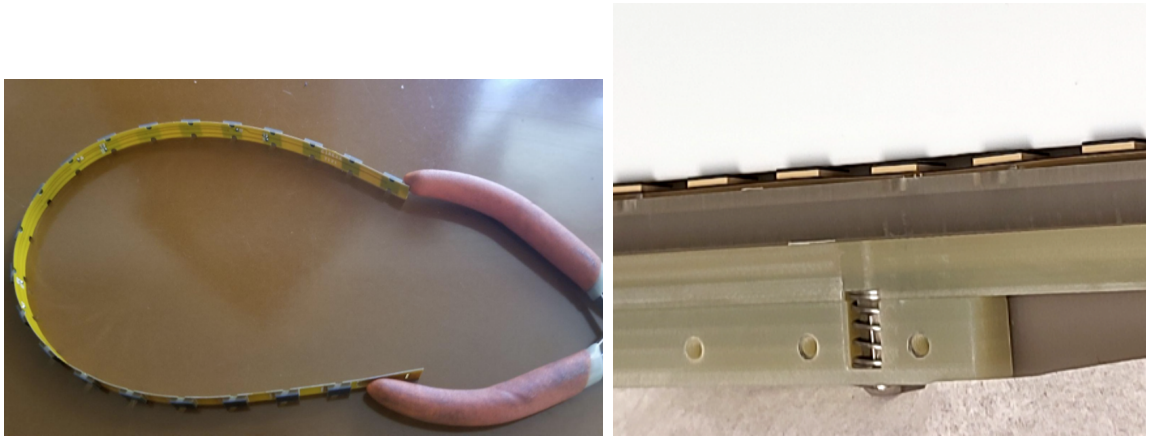

Figure 1.10: 20 SiPMs mounted to flexible PCB (left). Flexible PCB positioned against a dummy WLS plate (white block) with spring-loaded dynamic mount (right).

The required PDE for the PD modules is 2% with a target value of 3%, similar to the best achieved by the FD1-HD X-ARAPUCA [?, ?, ?, ?]. Measurements of PDE have not yet been made on full-sized FD2-VD PD modules but the fundamental design of the X-ARAPUCA is the same as for FD1-HD, so we expect similar performance. Nonetheless, there are differences that directly affect the PDE, most significantly the ratio of photosensors per light collection area is reduced by a factor of 2.4 compared to FD1-HD. Simulations indicate that this factor is compensated for by the more efficient WLS plates, spring-loading of the SiPM to WLS plate mounting to ensure mechanical contact, and reflective X-ARAPUCA frames. An additional enhancement may come from inclusion of light-concentrating cutouts in the edge of the WLS plates that simulations indicate increases the photon collection efficiency - validation studies will be completed prior to design baselining in summer 2023.

1.4.1 Cathode Modules HV Discharge Protection

Having the cathode modules mounted in the cathode plane exposes them to a risk of damage from a discharge event of the -300 kV HV system.

Two independent studies, one at Brookhaven National Laboratory (BNL) and one at Fermi National Accelerator Laboratory (Fermilab), agreed that the original design presents an unacceptable risk of damage to the X-ARAPUCA modules' electronics from a discharge, especially for the configuration in which multiple modules share power and signal, but that an open faced conductive enclosure around the SiPM flexible PCBs and readout cables, together with a complete enclosure of the cold readout electronics, provides sufficient risk mitigation.

As a result of these studies, the X-ARAPUCA module design has been modified to include a three-sided Faraday cage composed primarily of copper-clad FR-4 surrounding the SiPMs, flexible readout boards, and readout cables for all PD modules. Additionally, the readout electronics, and PoF in the case of the cathode mount modules, are enclosed in the Faraday cage. Details of this cage can be seen in Figure 1.11. The opening in the Faraday cage is $593.4 \times 593.4\,\mathrm{mm}^2$, matching the coverage of the dichroic filter windows.

This design will be tested and improved in test benches that will emulate the cathode discharge, with progressively increasing charge injection amounts to identify weaknesses. In FD2-VD Module 0 we will test the design on both shared/distributed power and signal system and independently powered X-ARAPUCAs. At the end of the FD2-VD Module 0 run, discharges will be induced from maximum cathode HV.

The final design will be validated in a cold box run in in advance of the Production Readiness Review."

1.4.2 Membrane Modules Suspension System

The membrane-mount portion of the PDS is composed of 20 columns of 8 PD modules on each of the two long walls of the cryostat, plus 2 columns of 8 PD modules on each of the two short walls, for a total of 352 modules. Each PD column is supported by two suspension lines. The suspension lines are made of three connected stainless steel pieces: a top rod bar (5 mm diameter, 3.7 m length) fixed on the cryostat roof, a central tube (12 mm diameter, 6 m length) in the central part of the detector, and a bottom rod bar (5 mm diameter, 3.7 m length) fixed on the cryostat floor. The top and bottom rod bars have eye bolts to be fixed on the M10 membrane bolts welded on the cryostat. The central tube has a larger (12 mm) diameter in order to avoid inducing large field gradients in the high voltage region near the cathode plane. The central tube is fixed between the two rod bars by shackles. There is a jaw to jaw straining screw and spring on the bottom rod bar, in order to compensate for differences between nominal and real line dimensions (75 mm adjustment range), to pre-load the spring, and to absorb the thermal expansion.

Each PD module has four attachment points, two on each suspension line, as shown in Figure 1.12 (left). The fixation points are made of wire rope grips pre-positioned along the 5 mm rod bars. Figure 1.12 (right) shows a zoomed image of one fixation point. Signal cables are routed along the rod bars toward the cryostat roof and floor, and then exit on the BDE cables tray. The estimated

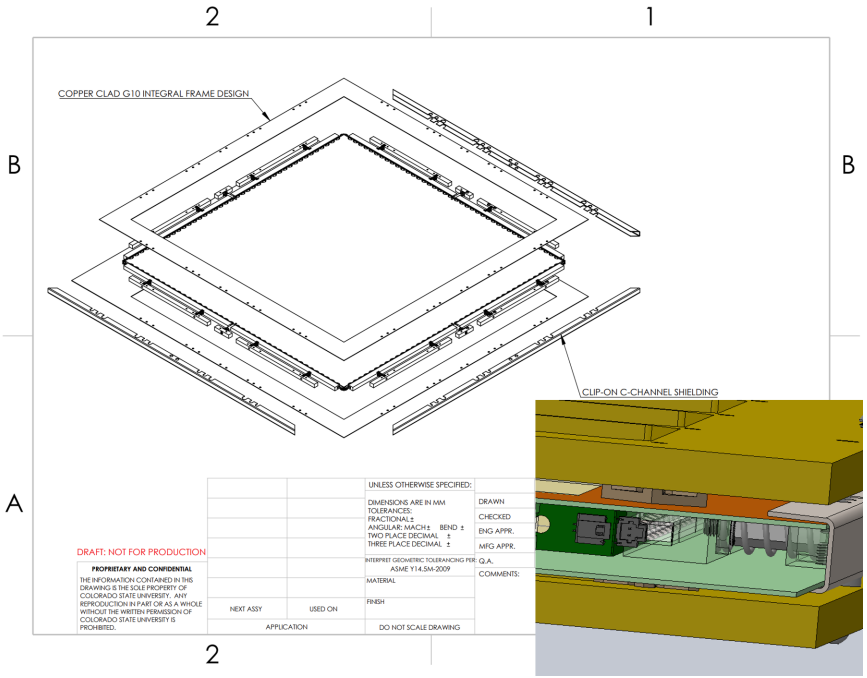

Figure 1.11: Copper-clad G-10 frames and formed stainless-steel external covers provide a 3-sided discharge shield for SiPMs.

weight of each PD module column, including 8 X-ARAPUCA modules, electronics, cables, fixation elements, and rod bars/tube lines, is about 110 kg. Several prototype suspension lines have been produced.

1.5 PDS Module Signal

1.5.1 Silicon Photosensors

The photosensors of choice for the FD2-VD are SiPMs. This choice is driven by the use of the X-ARAPUCA as the underlying technology for photon collection and the experience leveraged from the FD1-HD module development. The sensors developed in collaboration with the two main vendors of cryogenic SiPMs (Fondazione Bruno Kessler (FBK) and Hamamatsu Photonics (HPK)) fulfill the sensor specifications listed in Tables 1.1 and 1.4. Several candidate devices from these vendors have undergone extensive evaluation by the DUNE team over several years.The typical breakdown voltage for Si-photosensors at cold temperature is in the few tens of volts (~ 42 V for Hamamatsu MPPC and ~ 27 V for FBK SiPM). They will be operated at +3 to +5 V overvoltage, with a typical PDE at room temperature of 45% at 430 nm.

The SiPM development needed for the FD2-VD PDS was modest. Thanks to the experience gained in the construction of FD1-HD Module 0, we know that the failure rate is well below 0.5% and the dark count rate is marginal compared with the expected contribution from ^{39}Ar and other radiological backgrounds[7].

[7]Our background simulation (where ^{39}Ar is the dominant contribution) yields a flash rate of about 200 kHz for a flash reconstruction threshold of 3.5 photoelectrons. This is much larger than the flash rate induced by SiPM dark counts alone, and for the same 3.5 PE threshold.

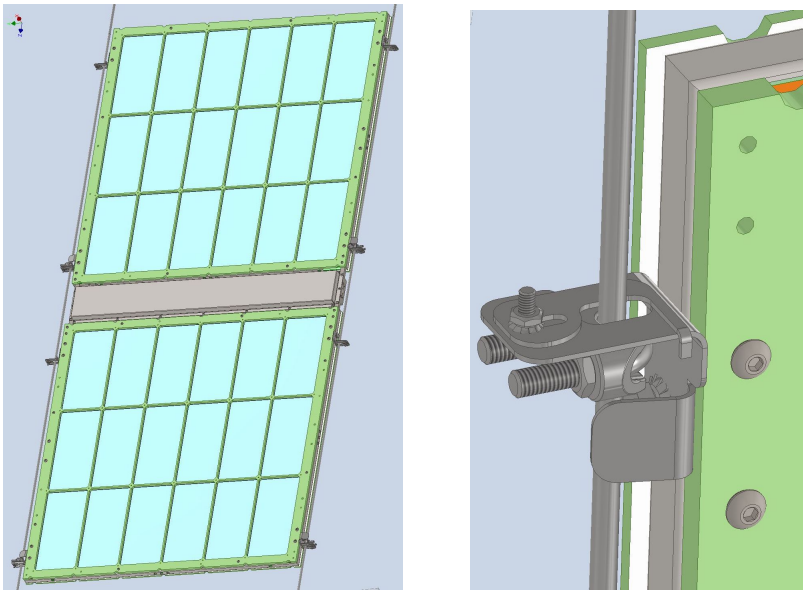

Figure 1.12: Fixation system for membrane-mount PD modules. (Left) Each X-ARAPUCA module is supported using four fixation points on two vertical suspension lines. (Right) Detail of one fixation point.

For optical coupling of the SiPMs to the WLS plate, both gluing and non-adhesive positioning were investigated. The results indicate that a spring loading system (see Section 1.4) provides an optimal solution. This solution was successfully validated in laboratory test-stands and during the cold box tests. The associated risks related to the thermal stress are mitigated by the flexible boards that host the SiPMs.

The baseline SiPMs choice is to use the S13360-5075HD-HQR (HPK) for the membrane modules and the NUV-HD-CRYO triple-trench (FBK) for the cathode modules. This solution benefits from the lower operating voltage of the FBK sensors to be biased by the PoF. Both types of sensors have been tested with the PoF system and achieved the expected performance.

As a consequence, the choice of SiPM models is mostly driven by cost-effectiveness and the performance of the cold electronics described in Section 1.6. The SiPMs do not represent a significant risk source for the design of the FD2-VD module.

1.5.2 Signal Ganging

The PD module SiPMs are mechanically pressed against a WLS plate and electrically connected to a flexible Kapton(R) PCB where 20 SiPMs are passively ganged to sum their electrical response. Summed signals from four flex PCBs are fed into the amplifier stage (active ganging, biased at +5 V), so a single electronic channel provides a readout of the combined response of 80 ganged SiPMs; there are two such channels per X-ARAPUCA. Both passive and active ganging stages are cold. This double-stage ganging solution, adopted for both cathode-mount and membrane-mount modules, represents an extension of the scheme adopted for the FD1-HD PD electronics where eight boards of six SiPMs are summed in a single-stage cold amplifier. Commercial components are used for the ganging signal conditioning circuit.

A flexible PCB is host to the passive ganging of 20 SiPMs of the FD2-VD PDS. Five groups of four SiPMs connected in parallel are connected in series, as shown in the equivalent circuit of Figure 1.13. advantage of allowing all the SiPMs to be biased at the same voltage while keeping the overall capacitance of the system low, thus ensuring a short This circuit has the advantages of ensuring the same potential on the surface of the SiPMs, and a small capacitance, hence a lower noise and generally faster response time. The ganged signal is read in differential mode in order to increase the S/N ratio.

Figure 1.14 shows four flexible PCBs ganged to make a single PDS channel (there are two such channels per module) that have been used successfully in the CERN cold box.

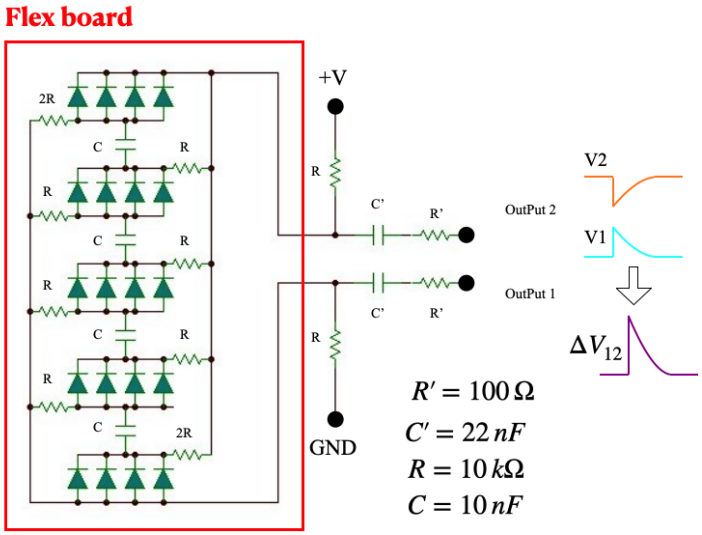

Figure 1.13: Equivalent circuit for the passive ganging of 20 SiPMs of the FD2-VD PDS.

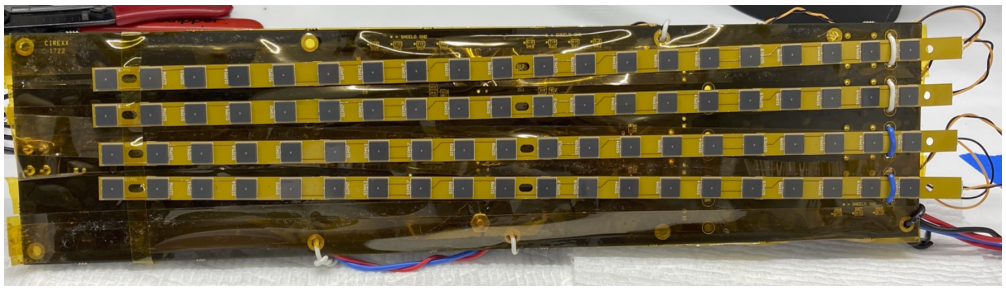

Figure 1.14: Four flexible boards with the 80 ganged SiPMs of a single FD2-VD PDS channel. The X-ARAPUCA light collector to which the four flexible boards are coupled is not shown in this figure.

1.6 Sensor Biasing and Signal Readout

1.6.1 Membrane Mount Modules

The FD2-VD design calls for 56,320 SiPMs and 704 signal transmission electronics channels (two signals per light collector module) to read out membrane mount modules.

The membrane-mount X-ARAPUCAs and associated readout electronics are at ground, so the readout solution developed for FD1-HD PDS, with power and signal transmitted over conductive cable, is a viable solution with minor changes and is adopted as the reference design. In parallel, a study is in progress to determine whether a more effective solution is to adapt the board containing the signal summing and amplifier stage developed for the cathode modules for use with the membrane system; power and signal would be over copper for the membrane modules. This would have the benefit of maximizing the similarity for the first stage signal processing of the subsystems.

The warm electronics (DAPHNE digitizer), and associated interface to data acquisition (DAQ), are adopted from the existing FD1-HD PDS solution [**?**].

1.6.2 Cathode Mount Modules

The cathode-mount modules will float at the cathode HV, requiring power and signal transmission via non-conductive cables. Liquid immersion, low temperatures, long maintenance-free lifetime, and HV isolation requirements combine for a particular challenge for the electronics.

1.6.2.1 Power-over-Fiber for Active Devices on the Cathode

Power-over-fiber (PoF) is a power delivery technology that delivers electrical power by sending laser light through robust, lightweight, non-conductive optical fibers to a remote photovoltaic receiver or photovoltaic power converter (PPC) to power remote sensors or electrical devices. This innovative technology provides three major benefits: (1) noise immunity, (2) voltage isolation, and (3) spark-free operation.

The current FD2-VD design consists of discrete PoF units that include a laser transmitter module on the warm side, a fiber link, and a PoF receiver on the LAr side. Figure 1.15 shows the basic block layout of a single PoF system. The laser transmitter is made of photonic power modules (PPMs), which are laser modules with fiber pigtails. The fibers are passed through a bearing sensor wire compression seal (BSWS) rubber cork feedthrough. The PoF receivers, called PPCs or optical photovoltaic converters (OPCs), deliver power to readout electronics and bias generation circuits.

The first silicon-based transmitter control unit (PPM module) consisted of a switching power supply, laser interlocks, controls and five Class 4, 971 nm wavelength, laser transmitters that each had fused fibers. This compact power housing unit is shown in Figure 1.16 and has been fully tested. A final, improved, design of the transmitter module that includes both local system communication capability and remote control is underway. An improved system will be deployed that includes eight, 2 W power capable and 808 nm wavelength, gallium arsenide (GaAs) lasers per control unit; the operational laser power target is 0.4 W. The control unit will have the same basic design, but the laser's compact footprint allows up to eight lasers per box.

The BSWS feedthrough leak rate with optical readout and PoF fibers has been tested at Fermilab in a stand-alone test bed with silicone potting by pumping against a small sealed volume to 10^{-6} Torr and conducting leak tests with a leak checker. The results were satisfactory (e-10 atm-cc/sec). The BSWS flange prototype with silicone potting has also been successfully tested in the NP02 cold box test bed, demonstrating the ability to reach the required LAr purity. The full-scale FD2-

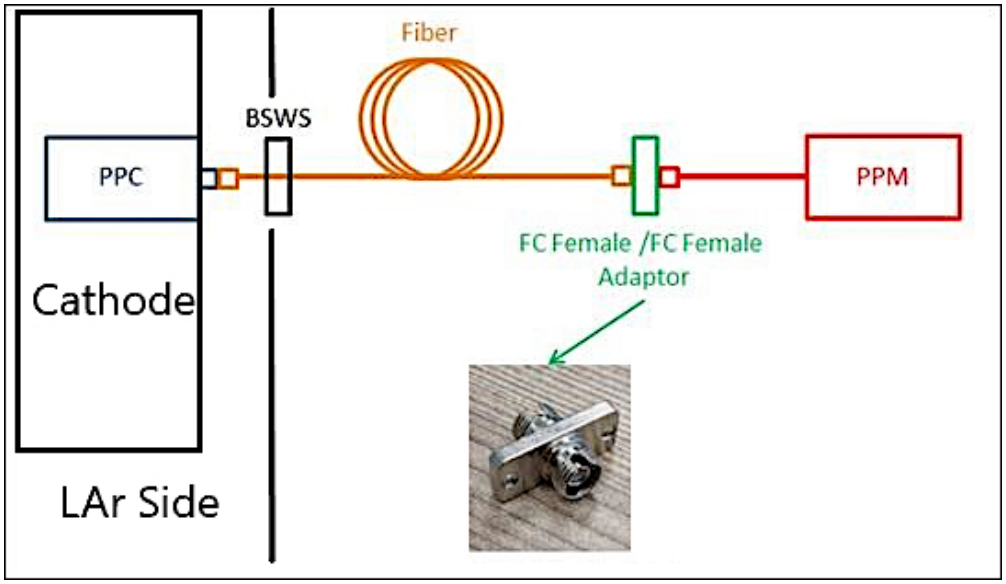

Figure 1.15: A block diagram of a single power-over-fiber (PoF) system with the vacuum feedthrough (BSWS) separating the LAr and warm sides.

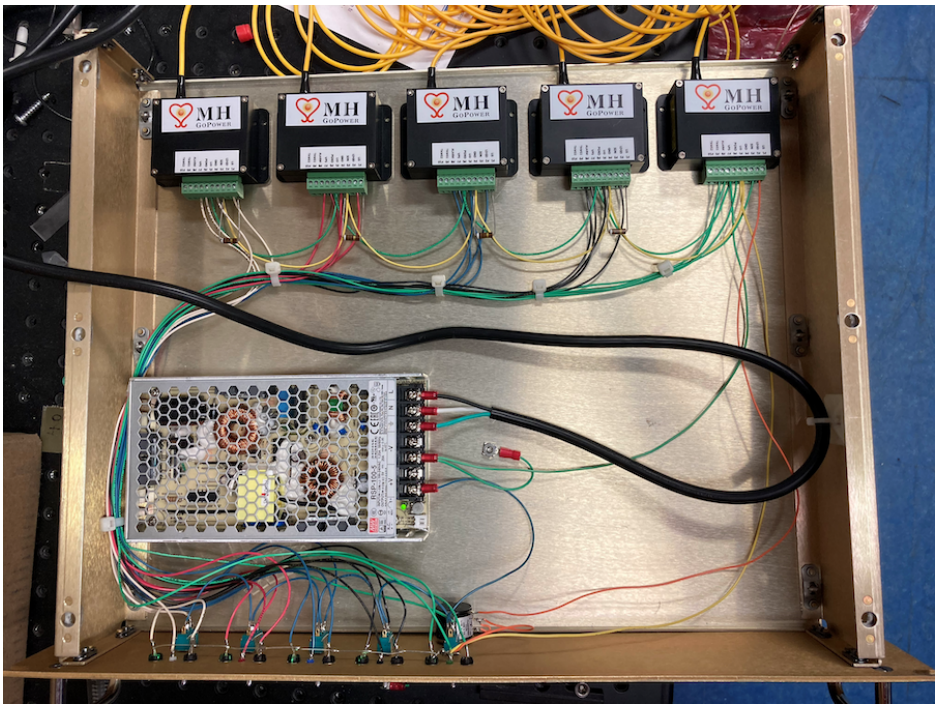

Figure 1.16: Photograph of the fully tested PoF transmitter module showing five 971 nm lasers.

VD PDS flange with epoxy potting will be tested in FD2-VD Module 0 allowing for final design validation well ahead of DUNE FD2-VD installation.

The readout electronics system voltage is 6 V and 450 mW power. To deliver the low voltage for the readout electronics, GaAs PPC receiver units [**?**] are deployed in parallel to provide sufficient current supply and redundancy. The voltage and power needs of the readout electronics must be closely monitored during cold box and FD2-VD Module 0 operation, as changes in power delivery requirements could imply changes to the PoF full system topology and a possible re-optimization for performance and cost. Compared to the silicon option, the GaAs PPC systems have higher efficiency at LAr temperatures at a similar, if not lower, cost. In LAr, the commercial silicon options deliver 200 mW at 12 V, while the commercial GaAs options deliver 200 mW at 6.5 V or 400 mW at 6.5 V. Specifications of the single PPC modules that have been considered are summarized in Table 1.7. Because of its higher efficiency, the GaAs technology is our chosen option for FD2-VD PoF.

Table 1.7: Power estimates for PoF cathode SiPM systems. Numbers refer to individual PPC modules.

Del. Power (W)*	**Type**	**Wavelength** (nm)	**Current** (mA)	**Voltage** (V)**	**Usable Power** (W)	**Eff.** (%)
0.6	GaAs warm	808	70	5.5	0.40	65
0.4	GaAs cold	808	30	6.5	0.20	50
0.8	Si warm	971	70	5.5	0.40	50
1	Si cold	971	16	12.0	0.20	20

* The power delivered is not all converted to usable power; e.g. for Si cold, the efficiency is about 20% in LAr.
** Each PPC module voltage can vary about 3%.

All PPC systems can be assembled in parallel or series sets, like batteries, in combination with Zener diodes, to achieve the required voltage and current. Figure 1.17 shows the basic block layouts of arranging PoF power systems. The PDS cathode-mounted module readout electronics motherboard, DUNE Cold Electronics Motherboard (DCEM), as shown in Figure 1.18, has been designed to accommodate the PPC units on G10 standoffs, with a heat sink with through-hole vias to provide power connection to the signal conditioning and bias generation circuitry. Up to four PPCs can be established in parallel on the motherboard PCB. The parallel mounting of three GaAs PPCs on the readout electronics motherboard is shown in Figure 1.18.

While sensor biasing and signal readout electronics will operate in cold, validation in warm conditions after installation is a requirement of the system, see Section 1.12.4. The SiPM bias is established with a DC-to-DC step-up converter to generate a bias voltage derived from the low voltage delivered by the redundant, parallel GaAs PPC units. The step-up converter is designed as a daughtercard to the readout electronics motherboard. The step-up converter can be tuned separately to the desired bias voltage for the SiPMs which is 20 V to 50 V in LAr depending on the SiPM type, see Section 1.5.1. A critical constraint for SiPM bias comes from the risk of high voltage discharge by the cathode; that is, the collapsing of the -300 kV on the cathode, which could occur due to arcing at the HV feedthrough. If not for this risk, SiPMs bias voltage could be shared among multiple X-ARAPUCAs, thus reducing the cost and complexity of the FD2-VD power distribution.

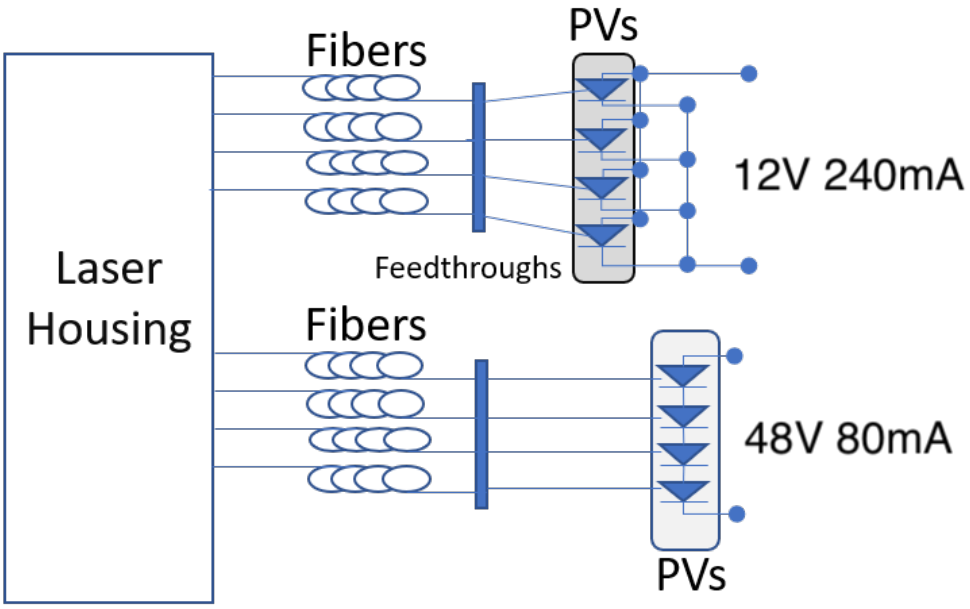

Figure 1.17: PoF receiver options. The photovoltaic (PV) components are housed in a small metal field cage-style unit called a PPC or OPC (optical photovoltaic converter). The series and parallel connections shown are for illustrative purposes only, assuming each unit is 12 V/80 mA. The actual number of photovoltaic components used will depend upon the semiconductor choice. For example, GaAs PPCs have lower voltage but higher current compared to silicon-based ones.

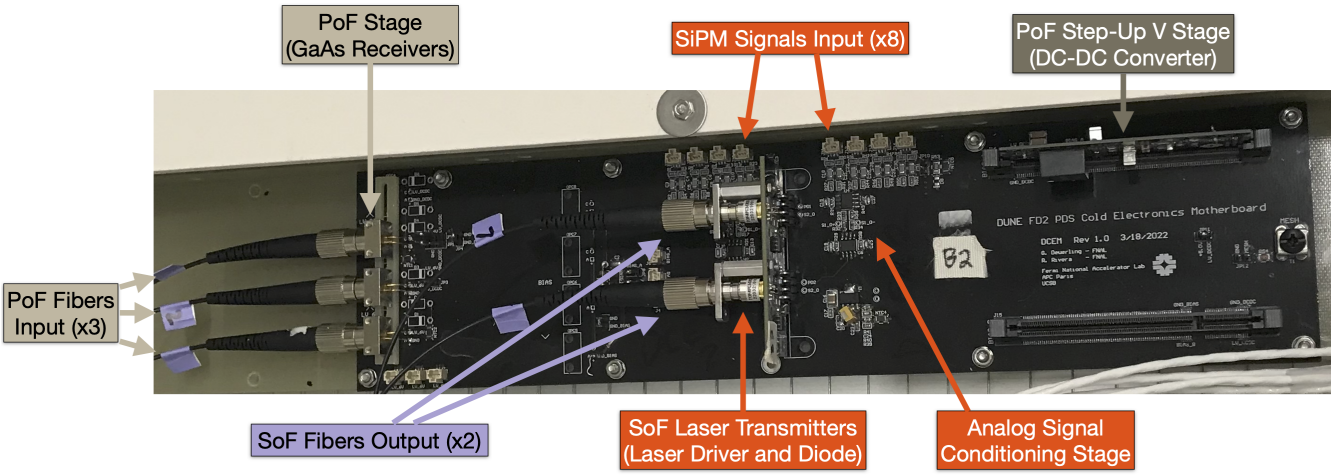

Figure 1.18: DUNE Cold Electronics Motherboard (DCEM) for the FD2-VD PDS. The labels indicate the main components. The board has been used in cold box tests at CERN.

However, as discussed in Section 1.4.1, a conductive distributed power system elevates the risk of damage to the readout electronics to unacceptable levels. Although a well-designed electrical shielding should provide sufficient protection, the safest option is to power each X-ARAPUCA independently in addition to shielding. To optimize costs, generating the bias through the use of PPC units in series was abandoned in favor of local bias generation using DC-to-DC step-up conversion.

A concern for the use of PoF in the vicinity of very sensitive photodetectors is related to photons leaking from the high intensity system. The selected black-jacketed fibers[8] were found to reduce the leakage of IR photons to undetectable levels using high-sensitivity thermal cameras. The PoF fibers are also routed through dedicated black polytetrafluoroethylene (PTFE) tubing (sloped and periodically slit to allow trapped gas to escape) and silicon potting may be employed at the terminations, providing further optical isolation.

Tests at the CERN cold box have shown that black-jacketed fibers and potted terminations are successful at preventing light leakage. FD2-VD Module 0 operation will confirm that the power delivery does not introduce an unacceptable background. More than one type of conduit, tubing, or braided sleeving will be deployed at FD2-VD Module 0 to compare background measurements for different solutions.

1.6.2.2 Signal Transmission

Analog optical transmission of the signal has been selected as the reference design based on numerous factors[9]. A similar parallel development by the DarkSide experiment showing promising results served as proof that analog transmission in LAr is possible, and therefore achievable within the constrained timescale of the development. The simplicity of design reduces risk associated with long-term cold qualification and affords a straightforward approach to PD module redundancy by increasing the number of analog transmitter channels per PD module.

As shown in Figure 1.19, the analog signals on the cathode are transferred, via a cold optical transceiver, over optical fiber to the external DAPHNE warm electronics for digitization and recording (the same system as the membrane modules). The FD2-VD topology calls for 51,200 SiPMs and 640 signal transmission electronics (two signals per light collector module) on the cathode.

Commercial transceivers are operated and certified only for temperatures greater than 233 K. Converting electrical signals to optical signals at LAr temperatures is thus recognized as a critical aspect of the readout of the PDS. Analog optical transceivers have been developed to operate at such temperatures previously [**?**]. In particular, the DarkSide Collaboration has developed a prototype transmitter for their experiment that shows satisfactory results [**?**].

An analog optical transceiver has been developed for FD2-VD. These transceivers are based upon commercially available discrete analog components, and the light source can be either a LED or a laser. A laser is used in the FD2-VD PDS, owing to its higher optical output efficiency in cold. Compared to DarkSide, the FD2-VD optical driver has no major radiopurity constraints but must

[8] MH GoPower 62.5 μm core diameter, 1.5mm OD, 40 m length, black PTFE coating.

[9] A digital optical transmission was investigated but could not be validated on the appropriate timescale.

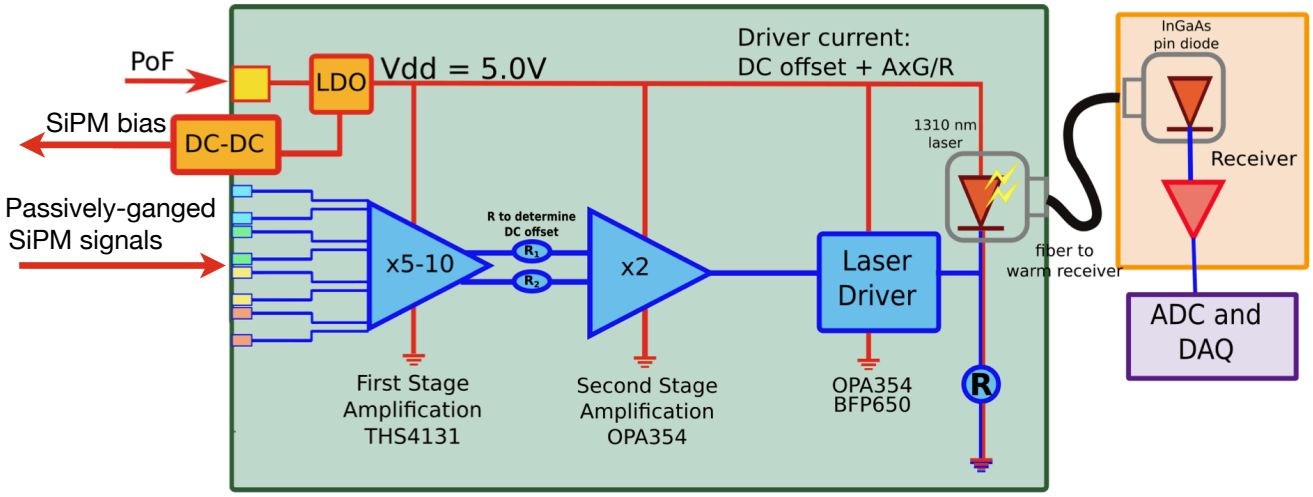

Figure 1.19: Readout electronics for cathode-mount PD modules - optical transmission of the analog signals to digitizers outside the LAr cryostat. The green box represents the cold readout components for one analog readout channel. The differential input on the left of the figure corresponds to 80 ganged SiPMs, hence two analog optical transmitters and two receivers per PD module are required.

serve a detector with a larger dynamic range. The design aims to reduce risks by implementing a minimum topology of discrete components that are known to have adequate behavior in cold, while attempting to match as well as possible the dynamic range of the signals coming from the X-ARAPUCA and minimizing power consumption.

The signals of each analog channel (80 SiPMs) are first amplified (signal shaping stage), then converted to a current signal (laser driver). Both stages are based on high-bandwidth operational amplifiers. The bandwidth of the transmitter circuit is one of the key aspects for properly transmitting the ganged signal of the SiPMs. With a rise time of around 50 ns, a bandwidth of at least 20 MHz is desirable in order to transmit the signal without significant deformations. In addition, the expected signal level for the single photoelectron is about 30-50 μV and hence requires amplification on the transmitter board. An appropriate balance between gain and bandwidth must be reached, given that a configuration with larger gain reduces the bandwidth capabilities of the circuit components.

Although it has been found that operation in cold reduces the performance of the driver with respect to operation at room temperature, an adequate bandwidth of 50 MHz in cold has already been achieved. The circuit drives current through an edge-emitting laser coupled to an optical fiber. Edge-emitting lasers show satisfactory behavior, with a threshold lasing current reduced to only a few milliamps in cold and with good linearity.

The linearity of the electrical-to-optical conversion and transmission for the analog signals in the dynamic range of expected signals is a crucial feature of the SoF system, and has been tested in detail with satisfactory results. Commercially available Fabry-Pérot laser diodes have been shown to work well as an optical signal source at cryogenic temperatures, with a lower threshold current in

cold and the same efficiency as in warm across its range of operation. The custom high bandwidth laser driver with fixed DC offset, to set the working point of the laser diode just above its threshold current in cold, enables the laser to efficiently operate in linear regime. The response of a sample of Fabry-Pérot laser diodes during acceptance tests in cold is shown in Figure 1.20.

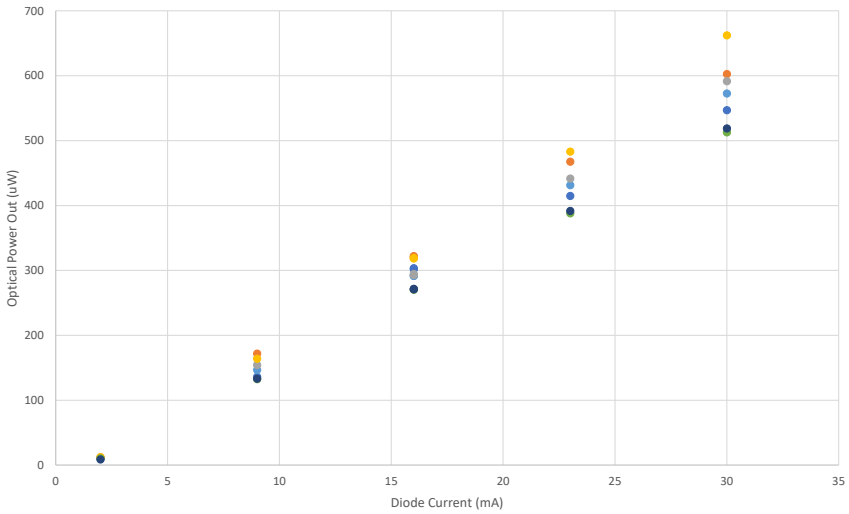

Figure 1.20: Linearity of response for a sample of six Lasermate Fabry–Pérot laser diodes from acceptance tests in deep LAr at Fermilab Proton Assembly Building (PAB). The optical power transmitted through the fiber is shown as a function of excitation input current (2.1 mA threshold). This test is for 500 µW devices over 40 m of 62.5 µm diameter multimode fibers, and read out via an optical power meter.

An annotated photograph of the DCEM is shown in Figure 1.18. One such board per X-ARAPUCA will be used. As shown by the labels in the figure, this single integrated board operating at LAr temperatures includes circuitry for PoF, analog signal amplification and conditioning, delivery of SoF and SiPM bias.

Power dissipation from the DCEM is within the specification from the HV group that limits the heat load to less than 1 W/cm^2 in order to avoid bubbles. We estimate a power dissipation of 400 mW across the two, 50% efficient, PPC modules needed per X-ARAPUCA PoF. The local heat load from the PPC modules does not exceed 200 mW/cm^2 at any location, and is hence within specifications. The DCEM board itself uses an additional 400 mW of power, yielding a maximum local heat load of 130 mW/cm2, also within specifications. Total power consumption across the entire cathode mount X-ARAPUCA system is about 300 W.

At the other end of the signal fibers and outside the cryostat, the analog optical receivers will operate at room temperature. The photodiodes to be used are InGaAs, since they have the optimal sensitivity to the 1310 nm light being used in the transmitter on the DCEM. The radius of the photosensor should be well adapted to the fiber core diameter; currently 300 μm is planned, since it would be appropriate for any of the fiber core diameters used, and it is a commercially available standard size. These devices have a responsivity[10] power-to-current conversion that depends on the incident light wavelength; for 1310 nm light this is close to 0.8 A/W.

[10]Output signal (typically voltage or current) of the detector produced in response to a given incident radiant power falling on the detector.

The photodiode is followed by a fast, low-noise amplification circuit. A carefully selected high-gain transimpedance operational amplifier is the basis of this stage. The gain should be such that the smallest signals expected from the transmitter, the single photoelectrons (SPE), are correctly digitized by the ADC that follows. This is a 14-bit ADC currently used in the DAPHNE digital electronics board, with a 1 V maximum input. The goal is to adapt the gain of the entire transmitted/receiver path to achieve both a good S/N in SPE signals and the readout of large signals. The analog signal targets a 1-to-2000 photoelectron dynamic range, the upper bound being dictated by the range of signals expected in beam-induced neutrino events.

Simulations have been performed to determine the occurrence of ADC saturation events for such a dynamic range. ADC saturation within specifications was achieved, see Section 1.2. Knowing the DC level of the transmitter signal is important, since it allows for checking that the transmitter circuit is working and functioning correctly. For this reason, DC coupling in the receiver and digitizer stage is desirable.

A commercial solution for the analog signal receiver, the Koheron PD100, has been in use since the first prototype. Despite its excellent noise performance and robustness, its gain is too large to be used in combination with an analog-to-digital converter (ADC) like that in DAPHNE, and its power input saturation point of 600 μW is too low. An in-house receiver is being developed that will allow the receiver stage to be fully configurable and adapted to the specific needs of this application. It will also enable a cost reduction in the final construction, and will better integrate with DAPHNE. The final design will be installed in FD2-VD Module 0, final optimizations will be made based on the installation experience during summer 2023. Since the receiver is external to the cryostat, it can be optimized even at a later time.

1.6.2.3 Power and Signal Fiber Routing

Figure 1.21 provides a 3D rendering of the routing of the PDS signal and power optical fibers for the cathode mount modules. From the module, they run internally to the cathode grid over to the edge next to the field cage vertical supports. From there, they run down to the cryostat floor into the cables trays provided for the bottom CRP detector electronics. These run up to the PDS flanges (Figure 1.22) on 32 of the penetrations that also carry feedthroughs for 4 CAT-6 cables, each of which serves 2 membrane-mounted PD modules, while the remaining 8 flanges will each carry 8 CAT-6 feedthroughs.

1.7 Light Response Monitoring and SiPM Calibration

The PDS will incorporate a pulsed UV-light system to calibrate and monitor PD response over time. The calibration system produces UV light flashes with a variable pulse amplitude, pulse width, repetition rate, and pulse duration. The calibration data recorded by PDS will be used to characterize and calibrate the PD gain, crosstalk, time resolution, channel-to-channel timing, and PDS stability over time. Examples of potential time instabilities to be monitored include dissolution of PTP coatings over time, or drifts in the power of the readout electronics lasers.

The system design, which has both warm and cold components, is very similar to that designed for the FD1-HD PDS and operated in ProtoDUNE-SP [**?**] where all the primary components of

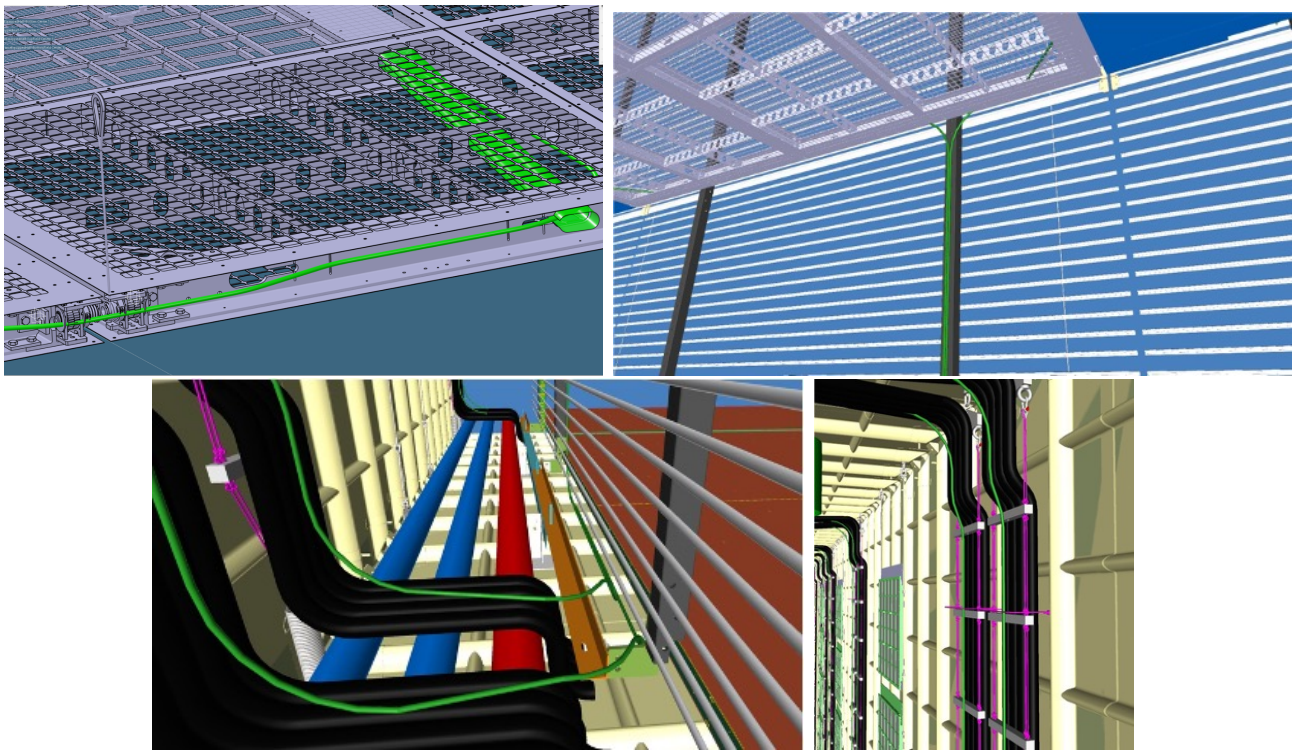

Figure 1.21: Cathode module optical fiber routing: Internal to cathode plane to the edge (top left); from the cathode plane edge to the field cage vertical supports then down to the floor (top right); (bottom left) transfer into bottom detector electronics cables conduit on the membrane walls; up the membrane walls and over to flanges on the cryostat top.

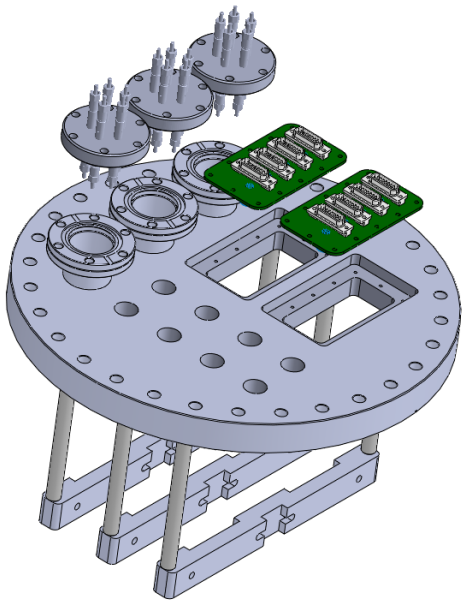

Figure 1.22: PDS flange with 3 feedthroughs for light response monitoring fibers, (top-left), 8 feedthroughs for fibers for cathode-mounted PDS modules (left), and feedthroughs for CAT-6 cables (right). Of the 40 flanges, 32 will have 4 CAT-6 feedthroughs, with the remaining 8 flanges having 8 CAT-6 feedthroughs as shown.

the system have been validated. A significant difference between ProtoDUNE-SP and FD2-VD is the typical distance between the point-like light source locations in the cold volume and photon detectors. However, illumination of a large area (6×6 m^2) of PMTs from a fiber placed at the top of the field cage in ProtoDUNE-DP demonstrated that there will be sufficient intensity for these longer distances.

Based on ProtoDUNE-SP prototyping and operational experience, the system hardware for FD2-VD calibration and monitoring system consists of both warm and cold components.

Fibers with diffuse fiber-end points mounted on the support structure around CRPs' perimeter above the field cage strips and at locations behind the field cage strips will serve as point-like light sources, used to illuminate the PDs mounted at the cathode and on the cryostat membrane walls. Quartz fibers transport light from the optical feedthrough (at the cryostat top) to the diffuse fiber-end points. In this configuration the light emission points are about 6.5 m away from the cathode surface. Warm components of the system include electronics boards with controlled pulsed-UV source (currently 275 nm and/or 365 nm) and warm optics. Cold and warm components are interfaced through an optical feed-through, optimized for the number of calibration fibers and for the size of the cryostat flange. Figure 1.22 illustrates the top, horizontal flange, which provides eight fiber feedthroughs each serving up to eight PoF and SoF fibers for one cathode-mount PD module, three optical feedthroughs serving up to 15 Response Monitoring System diffusers.

Most of the design of the FD1-HD calibration system will be reused for FD2-VD. The primary differences with respect to the ProtoDUNE-SP system are the number and location of the fibers and its diffuse end-points, the lengths of the optical fibers, and the addition of a monitoring photodiode within the LED light source. The diffuse fiber end-points will be attached at support structure around the CRP perimeter at locations indicated in Figure 1.23. Each of these point-like diffuse sources will illuminate the cathode and membrane-mount X-ARAPUCAs using pairs of fibers. In each pair, one fiber will be pointing inward toward the cathode-mount PD modules and one fiber will be pointing outward toward the membrane-mount modules. The calibration system will have 24 pairs close to the top CRPs, and another 24 pairs closer to the bottom CRPs. These fibers run to the flanges at the top of the cryostat, where the electronics modules with light sources will be located.

The optical fiber, fiber routing scheme and optical feedthrough components, as well as light source electronics, have been designed for FD1-HD and will be tested in FD1-HD Module 0. For FD2-VD, the diffuse light point design and distribution will be optimized for light coverage of PD units located across the cathode and on the cryostat membrane walls. Design options include use of a bare fiber end as a diffuse light point, and/or installation of a small quartz light diffuser at the fiber end to provide a more uniform illumination (see Figure 1.24).

The FD2-VD Module 0 will be used to validate the design and evaluate the performance of the calibration system for FD2-VD. The FD2-VD Module 0 system provides ten calibration fiber-end diffuse ends. Calibration light is diffused from six light emission points attached to upper CRPs support structure with four diffuse-end points to illuminate cathode PDs, and two diffuse-end points to illuminate membrane wall PDs. There are four light emission points attached to lower CRPs support structure with two diffuse-end points to illuminate cathode PDs, and two diffuse-end points to illuminate membrane wall PDs. A test will be performed to determine if the

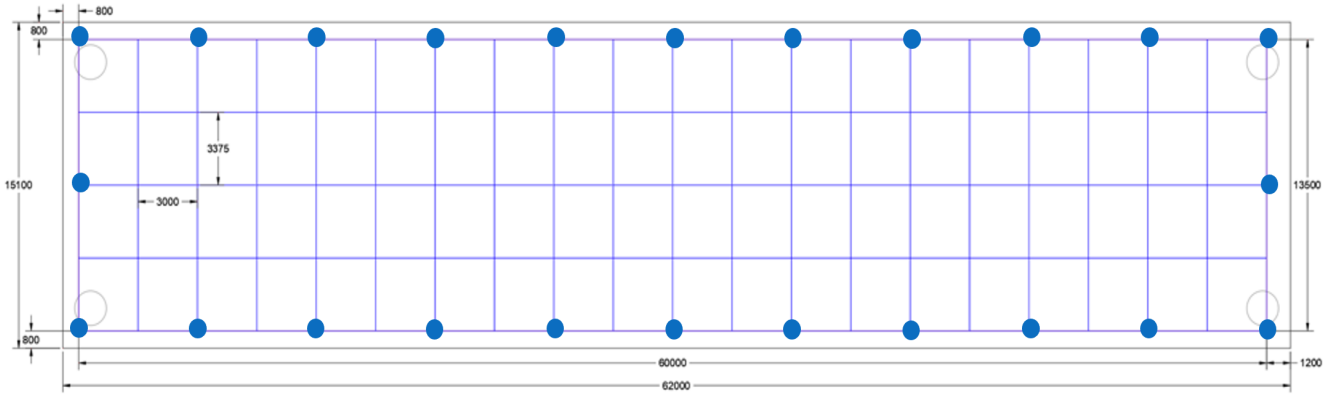

Figure 1.23: Location of the calibration system optical fibers with diffusers at the ends. They are installed along the perimeter of the CRP (viewed from above) and illuminate the PDs mounted on the cathode and cryostat walls.

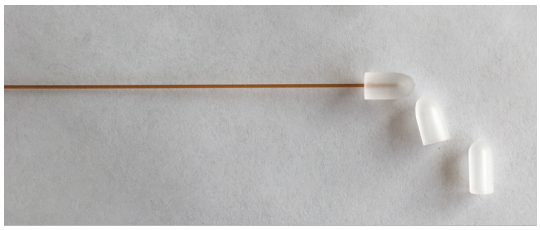

Figure 1.24: Diffuser (6.0 mm diameter) attached to bare fiber (0.7 mm diameter).

light emitting points at fibers-end may diffuse light via either bare fiber-end or with the designed diffuser unit attached to it as shown in Figure 1.24. One of the top fiber-end emission points will be instrumented with the diffuser unit.

Multiple quartz fiber types will be tested for the light transport and diffusion characteristics in FD2-VD Module 0: two types of fibers with different solarization resistance of the quartz core (200 and 400 μm core diameter), and the third type already selected for FD1-HD Module 0 (600 μm core diameter, which is expected to have a negligible solarization effect). Two fiber jacketing options are considered depending on fiber installation route constraints: PTFE jacket, or stainless-steel jacket.

The system has no active components within the cryostat. The active system component consists of a 1U rack-mount light calibration module (LCM) at warm temperature. The LCM electronics system generates light pulses that propagate through a quartz fiber-optic cable to the diffusive fiber-end to distribute the light across the PDs. The current calibration module design consists of a field programmable gate array (FPGA) based control logic unit coupled to an internal LED pulser module (LPM) and an additional bulk power supply.

The LPM uses multiple digital outputs from the control board to control the pulse amplitude, pulse multiplicity, repetition rate, and pulse duration. Analog-to-digital converter (ADC) channels internal to the LCM are used to read out a reference photodiode used for pulse-by-pulse monitoring of the LED light output. The output of the monitoring diode is available for monitoring and

for normalizing the response of the SiPMs in the detector to the calibration pulse. Hardware components for the far detector (FD) modules will be costed based on the prototyping cost and expertise gained with FD2-VD Module 0.

Complementary to the monitoring system, a calibration of the absolute energy scale as a function of position within the detector will be pursued. The goal is to derive the position-dependent LY in the detector, in units of detected photoelectrons per unit energy deposit, from the data themselves. Several options are under consideration, including cosmic ray tracks, radioactive sources (at fixed positions or diffused into the LAr volume), pulsed neutron generators, and ionization lasers.

1.8 Design Validation

This section summarizes the results of the R&D and prototyping plan carried out for the FD2-VD PDS following the Conceptual Design Report and the on-going design validation program.

1.8.1 Xenon doping in ProtoDUNE-SP

A xenon-doping campaign was carried out in ProtoDUNE-SP a few months after an incident with a gas recirculation pump had let an unknown amount of air inside the detector volume. Oxygen and water were efficiently removed by the purification loop, but nitrogen cannot be removed by the purification filters. A residue of nitrogen ($\sim$ 5.4 ppm in mass) remained in the LAr with the result that the scintillation light was effectively quenched. Although it was not originally foreseen to do xenon testing in the presence of nitrogen contamination, its presence presented the opportunity to demonstrate light recovery due to xenon doping and a large scale.

The doping run consisted in doping argon with up to 18.8 ppm of xenon, in steps. The amount of detected light increased as a function of concentration up to around 16 ppm, after which the gain flattened. This trend was consistent across the three types of light detectors in ProtoDUNE-SP PDS. The results were corroborated by measurements taken with two prototype X-ARAPUCA detectors inserted for this run in the non-active TPC region behind one of the APAs. A paper on this work is in internal review.

Initial small-scale tests and the procedure used for ProtoDUNE-SP demonstrated that the doping of xenon and the mixing with argon must happen in gas phase, before condensation of the fluid. Indeed, since xenon liquefies at 165 K and solidifies at 161 K, creating a solution with liquid argon must be performed with extreme care, in order to avoid its freezing. Several mixing ratios were tested, showing that the Ar/Xe ratio must be above 10^3, to avoid xenon solidification on the walls of the argon condenser. This *freeze-out* effect can be easily observed since, at the highest xenon concentrations, the pipes of the condenser get clogged and the argon recirculation stops.

For ProtoDUNE-SP, the xenon injection point was placed on the gas recirculation system; on the line collecting the chimney boil-off, after the argon gas purification filter but some distance before the condenser. This allows for full mixing within the gas flow. The maximum xenon mass flow rate was set to 36 g/h, to be well within the Ar/Xe ratio limit mentioned above; this corresponds to 50 ppb/hour in the ProtoDUNE-SP detector. Based on a numerical computational fluid dynamics (CFD) simulation of the LAr flow within the ProtoDUNE cryostat, the xenon injected at this rate

is expected to be uniformly distributed in LAr within few hours.

Here we summarize the main results of the successful run:

- Since one of the two X-ARAPUCA detectors was fitted with a quartz window, which makes it insensitive to 128 nm photons, it is possible to disentangle the contribution of the xenon photons alone from the total emitted light. Comparison of the signal from the two detectors clearly shows that the amount of light above the quartz window cut-off, "xenon light", increases with xenon concentration. The ratio of the xenon-to-total argon light collected by the two detectors, as a function of xenon concentration, is shown in Figure 1.25.
- The data shows that the effect of xenon is simlar across the several detector technologies which are at different locations in ProtoDUNE-SP. This indicates good uniformity of the doping throughout the TPC volume. Time stability of the mixture is observed at the level of few weeks after the last doping event (afterwards, the run was stopped).
- Light attenuation curves show that the amount of detected light increases more further from the detectors, demonstrating the usefulness of the doping for very large volume TPCs (Figure 1.26). This is even more evident in a subsequent xenon-doping campaign in the ProtoDUNE-DP, which features a larger drift distance [**?**].
- In the ProtoDUNE-SP configuration, the increase of light with xenon concentration starts flattening out at around 16.6 ppm.
- No detectable deterioration of the charge collection performance, i.e., of the imaging capability of the TPC, was observed during the doping campaign.

In addition to the ProtoDUNE-SP run, ProtoDUNE-DP was partially emptied and refilled with the doped argon transferred from ProtoDUNE-SP. The amount of nitrogen was increased in order to reproduce the conditions of ProtoDUNE SP. The measurements taken in ProtoDUNE-DP also show an increase in the amount of collected light, which is becoming more and more evident with increasing distance from the detectors (due to the larger Rayleigh Scattering length). This result is published in the overall paper on the performance of the ProtoDUNE-DP light detection system [**?**].

The results of the two campaigns cannot be directly compared due to the significantly different TPC configurations and light collection technologies. However, both demonstrate that xenon doping will provide greater light yield uniformity and allow photon detection recovery from accidental nitrogen contamination for multi-meter drift-path TPCs.

1.8.2 X-ARAPUCA Module Optical and Mechanical Development

The X-ARAPUCA concept of the FD2-VD PDS module is the same as that of FD1-HD. Though the design benefited greatly from the FD1-HD development through to the final design, an R&D program was pursued in those aspects most impacted by the significantly different geometrical layout of the FD2-VD modules.

The development of the FD2-VD module focused on:

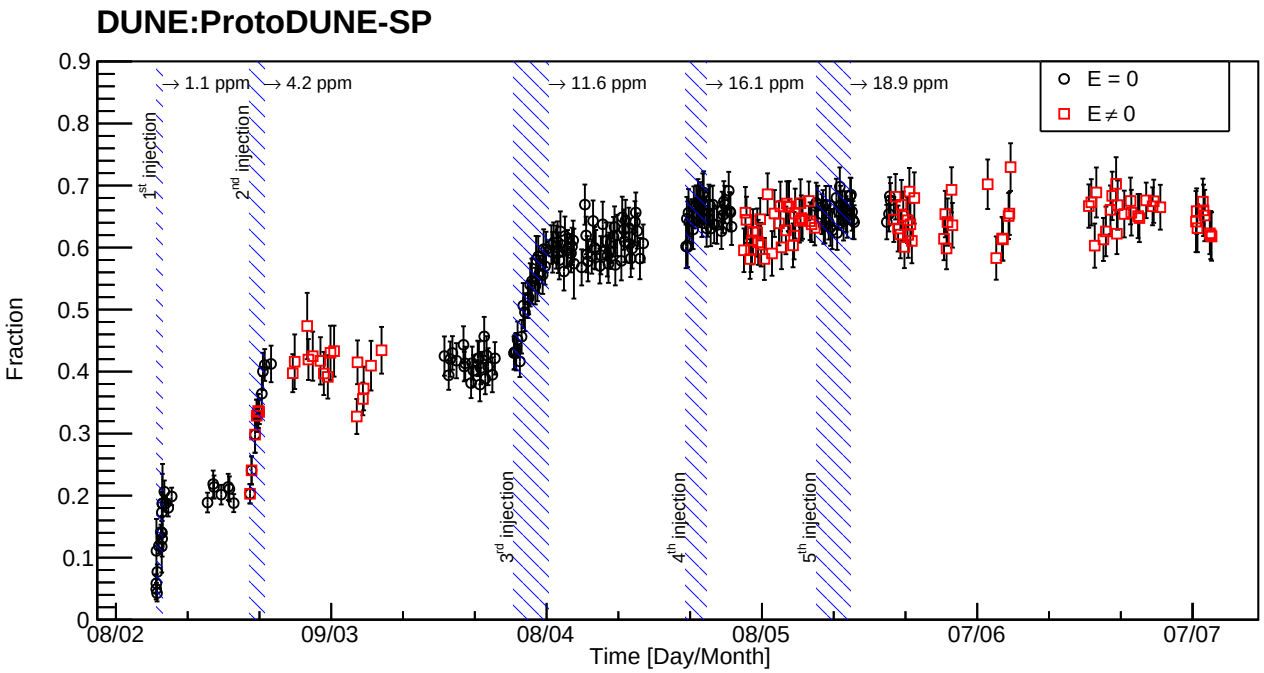

Figure 1.25: Fraction of light collected by the xenon light-only sensitive X-ARAPUCA in ProtoDUNE-SP, with respect to total light collected by the other device: $\frac{\text{Xe}}{\text{Ar+Xe}}$. The ratio increases with the doping concentration and reaches a plateau around 0.65 for xenon concentration greater than 16.1 ppm. The red points correspond to data collected with the nominal TPC electric field (500 V/cm), while black points refer to data with no electric field. Shaded areas indicate xenon injection periods.

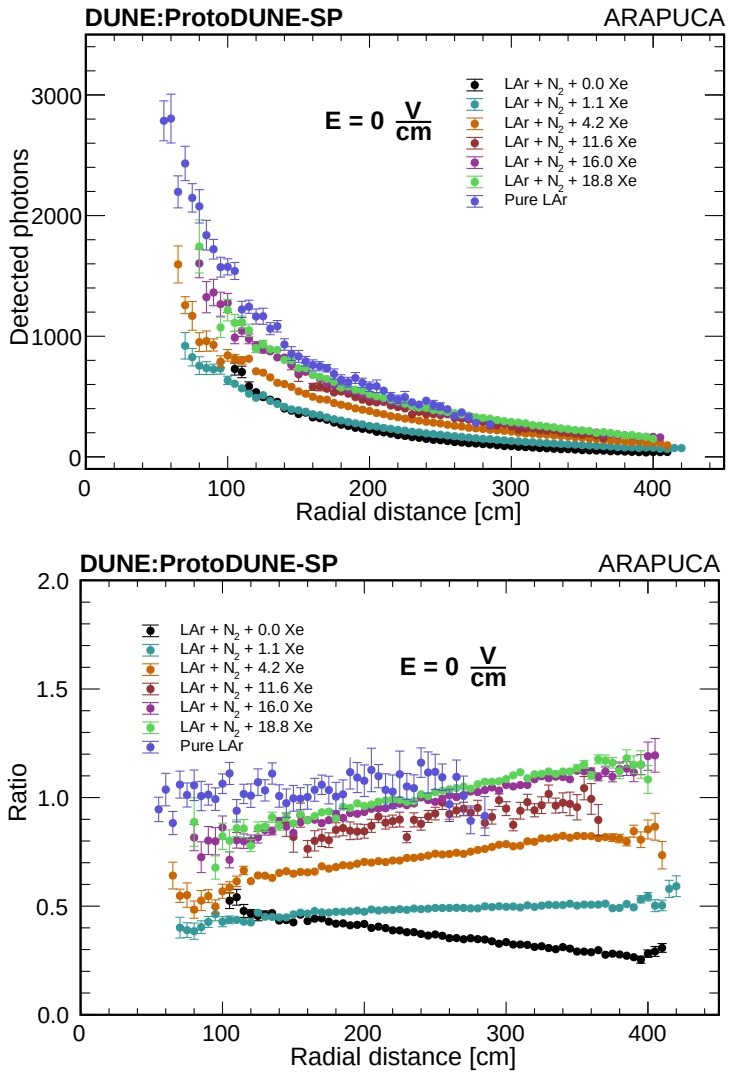

Figure 1.26: Light recovery is demonstrated through attenuation curves after xenon injection in the nitrogen-polluted ProtoDUNE-SP. Data collected with the non-beam side ARAPUCA. The left plot shows the collected light versus distance from the detector; the right plot shows the ratio of collected light with nitrogen (black points) and with nitrogen+xenon, with respect to non-polluted LAr (blue points). Data refer to runs with no active electric field. The right plot shows how the increasing concentration of xenon enhances light recovery further from the photon detectors.

- Production of large area WLS plates of $607 \times 607 \times 3.8$ mm^3 dimensions compliant with cryo-resilience, optical grade, and thickness requirements;
- SiPM mounting onto flexible kapton PCB (instead of rigid FR4 PCB pin coupled to FR4 routing boards) utilized for both the SiPM mechanical support and the signal routing;
- Spring-loaded mounting of the WLS/SiPM photon collector structure inside a G-10 frame, to compensate for their differential thermal shrinking (about 1%);
- Optimization of the dichroic filters optical density and reflectivity at specific angle of incidence (maximimized for 45deg, the average angle of the Lambertian emission angle distribution) and wavelengths;
- Development of larger size (202×97.5 mm^2 and 143.75×143.75 mm^2) dichroic filters to minimize the surface area of the non-active holder frame profiles of the dichroic filters.
- Optimization of PTP coating on large size filters;
- SiPM coupling via optical grade epoxy to a WLS plate forming an integrated readout structure;
- Laser cutting of the WLS tile edges with cutouts of rectangular/elliptical shape, to improve the photon collection as they exit the lightguide and to mitigate SiPM gluing.

1.8.3 Cryogenic PD Testing Facility for FD2-VD Module 0

In late 2022 a cryogenic facility was constructed at the Neutrino Platform facility at CERN EHN1 building to test full size X-ARAPUCA modules and read-out electronics, see Figure 1.27. This facility provides final functionality check and validation in cold prior to deployment in the FD2-VD Module 0 cryostat and detector integration. The 4×4 m^2 test area is located at CERN building 887/R-291 Salève side, in front of the ground floor PDS Lab barrack, where the assembly of the X-ARAPUCA PD modules is be performed.

A 70-cm diameter $\times$ 120-cm tall open air Dewar contains a (non-purified) LAr bath, which can be sealed with a custom-made lid that ensures light tightness and free exit for gaseous argon boil-off. A trolley with a winch allows insertion and extraction of a PD module. To minimize the usage of liquid argon and ensure safe warm-up and fast operation turnaround, a stainless steel box that can accommodate the X-ARAPUCA module is inserted inside the Dewar and filled with LAr.

At the end of a test, when extracting the module while it is still cold, nitrogen gas flowing under the box contained by a polyethylene skirt, prevents frost condensing on the modules. Cables and optical fibers routed via dedicated feedthroughs on the lid allow for cold electronics readout during test and calibration with a LED pulsed flasher installed inside the Dewar. Temperature sensors and a slow control system are used to monitor the LAr level and temperatures at different heights inside the inner vessel.

All 16 X-ARAPUCA modules for FD2-VD Module 0 were tested, and qualification data acquired, analyzed, and stored.

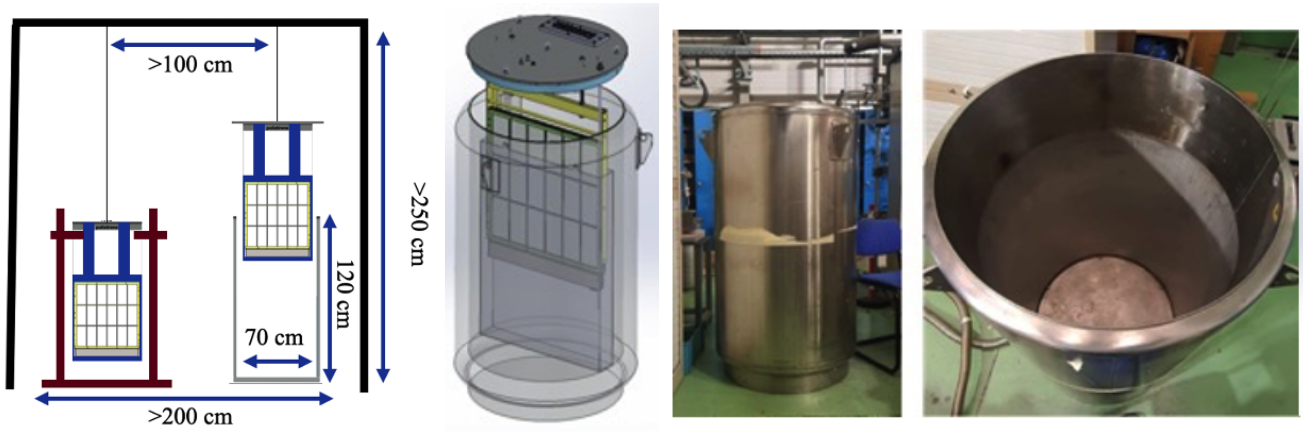

Figure 1.27: Schematic (left) and Dewar photos (right) of the mini-cold box at CERN, for testing X-ARAPUCA modules prior to installation in FD2-VD Module 0.

1.8.4 PD Module Validation

During 2021 and 2022, all the components were developed and prototypes fabricated. Integration techniques and procedures were developed and tested.

Fully-instrumented X-ARAPUCA modules have been tested both at the Proton Assembly Building at Fermilab, which serves as a test-bed for cryogenic electronics and PoF development, in a test facility at CERN commissioned in later 2022 (described in Section 1.8.3), and in the cold box demonstrator, in NP02 at CERN, starting in summer 2021 and continuing through to 2023, see Table 1.8.

Three prototype versions (X-ARAPUCA.V1, X-ARAPUCA.V2, and X-ARAPUCA.V3) have been deployed and operated in the cold box demonstrator, as can be seen in Figure 1.28. The V4 and V5 prototypes were validated in the EHN1 FD2 cold box ahead of FD2-VD Module 0 installation: these versions integrate different technologies of electronics shielding, SiPM-to-WLS coupling, and WLS edge shaping. An independent module mechanics design committee set up by the FD2-VD PDS consortium management evaluated the designs and down-selected from the two options (V4 and V5) to a single option (essentially V5) that is deployed in FD2-VD Module 0. These value engineering efforts are aimed at increased manufacturability, reduction of fabrication costs, and optimization for shipping.

1.8.5 Cathode-Mount Module Cold Electronics Validation

Numerous tests of the electronics developed for the SiPM signal read-out of the cathode-mount PD modules V1 to V5 have been performed in the cold box, starting from the earliest prototypes (Dec. 2021) to the latest fully integrated final design board (Dec.22-Feb.23 - DCEM board shown in Figure 1.18). In this section first results are reported on the read-out electronics response characterization validating the final design of the DCEM board.

For the analysis of the electronics response, a pulsed LED calibration system is implemented in the cold box. It consists of a board that drives a 310 nm LED flasher, into a quartz fiber ending into a light diffuser placed in the LAr bath inside the cold box. The intensity and the width of

Table 1.8: PD module prototypes.

Version	Description
V1	First full-size FD2 PD module. 3-sheet filter frame design, coil springs for pressing SiPMs against WLS plate.
V2	Changes primarily to dichroic filter frames, incorporating leaf springs to press SiPMs against WLS, Single-sheet filter frame with spring-loaded filter plates.
V3	Evolution of V2 design, making improvements to filter frame assembly.
V4	Final version of leaf-spring SiPM mounting design with spring-loaded filter windows in single-piece frame. Evaluated as part of Module-0 mechanical design process.
V5	Final version of coil-spring SiPM mounting design with Teflon washers mounting filter windows in single-piece frame. Evaluated as part of Module-0 mechanical design process.

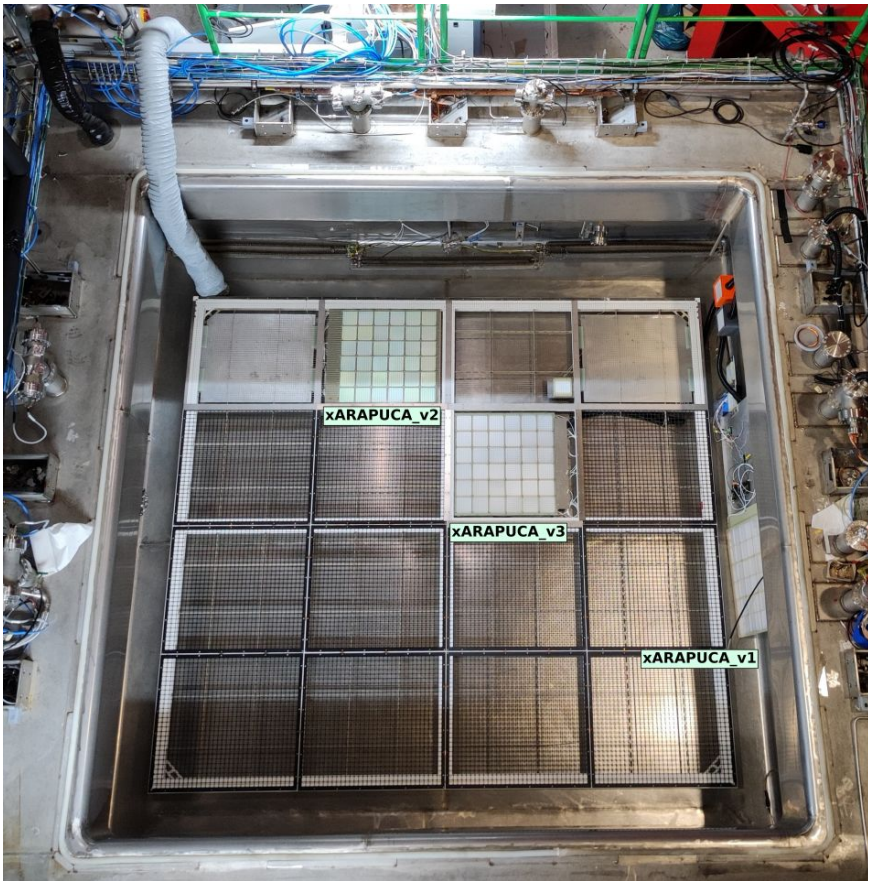

Figure 1.28: Top view of the cold box demonstrator at CERN, showing three X-ARAPUCA prototypes installed. The first prototype is mounted on the cryostat wall, while the second and third prototypes are mounted on the cathode.

the LED pulse can be selected, down to about 20 ns minimum duration.

The DCEM board in its final configuration is made of three main stages, the PoF stage (with two OPCs, optical-to-electrical power converter, and a bias circuit transforming the OPC low output voltage to the high SiPM bias voltage), the signal amplification and conditioning stage, and the 2-channel SoF transmitter (laser diode and its driver for signal transmission over optical fiber). The board, with input cable connections from the SiPM flex boards, is placed within a Faraday shielding metallic box along one side of the X-ARAPUCA module.

The first key milestone achieved is the demonstration of a signal-to-noise ratio (SNR) above the requirement of 4. Figure 1.29 shows the charge spectrum obtained with minimum LED pulse amplitude illumination, with peaks representing the charge distribution for 1-PE to 6-PE, above the first noise (0-PE) peak. From the multi-Gaussian fit, the ratio of the 1-PE peak position to the width of the 0-PE peak SNR=5.9 is obtained. This SNR is obtained operating the X-ARAPUCA module (V4) on the cathode at high voltage, during TPC operation. The DCEM read-out board is powered by PoF laser power via optical fiber and SiPM electrical signals are converted into optical signals and transmitted by SoF laser diode via optical fiber. Signal and noise levels were stable during the cold box run.

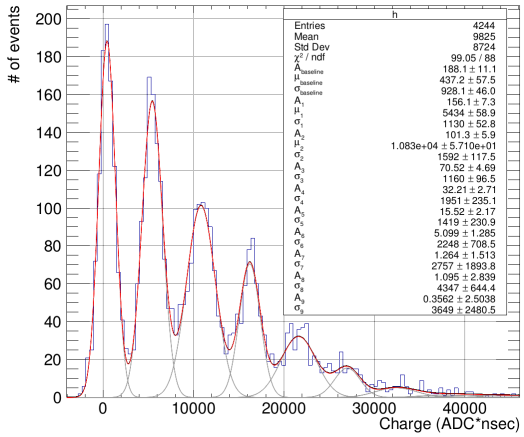

Figure 1.29: Photoelectron charge distribution for a full cathode module, obtained with the data from February 2023 cold box test with PoF and SoF. An SNR of $\sim$ 5.9 was obtained.

The impulse response function of the readout electronic chain, SiPM signal summing, cold DCEM analog signal conditioning and warm signal optical-to-electrical conversion (commercial Koheron PD100 board) and digitization, is obtained by $\sim$20 ns narrow LED flasher pulsing. Figure 1.30 shows the average of 500 signals obtained with fixed amplitude LED pulse. The relevant characteristics are highlighted on the plot, namely the rise time and discharge time measured between the 10% and 90% of the pulse amplitude, of 40 ns and about 400 ns respectively. The rise-time obtained is that expected from 80-ganged SiPMs, indicating that the bandwidth of the transmitter is adequate.

Linearity of the SoF electronics was first demonstrated with lab test-bench measurements over a limited range of signal amplitude, corresponding to few tens of PEs. Using data acquired at the cold box, it has been possible to evaluate the linearity of the entire readout chain, from the photosensor to the warm receiver, for a much larger dynamic range.

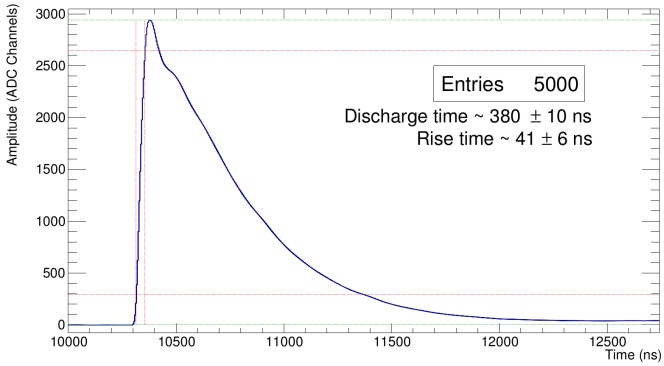

Figure 1.30: Average of 500 pulses obtained from the cathode modules. The rise time measured between 10% and 90% amplitude is $\sim$ 40 ns, while the discharge time is around 380 ns.

Signal waveforms were recorded with LED calibration flasher pulsed from minimum to maximum amplitude settings. The linear correlation between amplitude of the signal waveform (pulse height expressed in ADC counts) and signal waveform integral (after charge-to-PE calibration is applied) for various LED flasher amplitude setting is shown in Figure 1.31. The pulse amplitude of the recorded signals is limited to a maximum of about 1.5 V ($\sim$ 13000 ADC), since the warm receiver is saturated at this point. The linearity shown in Figure 1.31 demonstrates that the signal maintains the expected shape without distortions over the dynamic range of interest. A slight non-linearity of the LED calibration system signals appears at higher LED pulse amplitude settings that does not occur for scintillation signals from cosmics for all amplitudes. This residual non-linearity of the LED calibration system has to be taken into account.

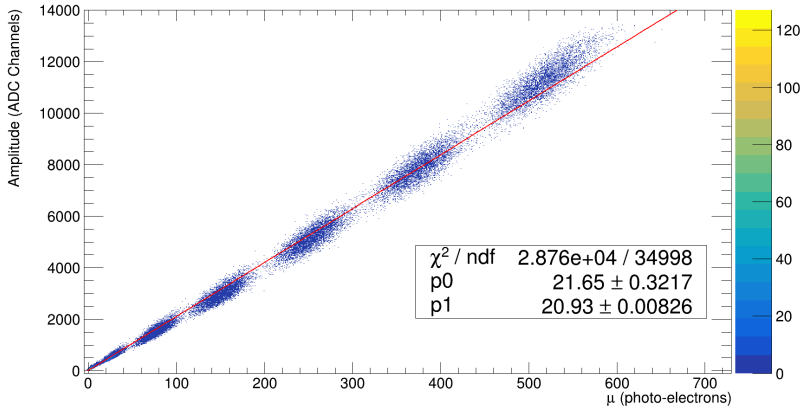

Figure 1.31: Linear growth of signal amplitude as a function of the number of PE, estimated from the integral of the SPE charge. The groups of data correspond to LED voltage levels. The saturation is due to the warm receiver's maximum input limit.

The full dynamic range was evaluated in a special channel of a DCEM board with lower light output also tested in cold box for V4 X-ARAPUCA module read-out, without the saturation limitation of the warm receiver (whose gain will be adjusted for the in-house receiver under development to replace the commercial Koheron board). The resulting measurement, going up to almost 2000 PE equivalent signal amplitude, is presented in Figure 1.32.

The X-ARAPUCA detectors have a very small, but non-zero, sensitivity to the 808 nm infrared

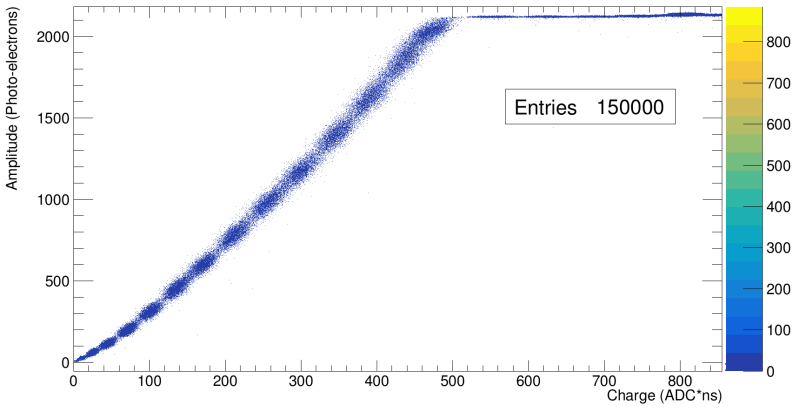

Figure 1.32: The dynamic range of the system has been demonstrated from the SPE level to over 2000 PE.

light of the PoF laser. This means that the PoF fibers and connectors at OPC receivers must be adequately shielded. Potential light leakage is effectively mitigated by potting the OPC receivers and connectors on the DCEM boards with electronic grade silicone paste and also by the metallic Faraday boxes surrounding the electronic boards. Light leakage from the PoF fibers becomes negligible when black jacketed fibers are bundled in the protective black tubes used for fiber routing from PD modules on the cathode to the feedthrough flanges at the top of the cryostat. Lab tests have demonstrated optical noise due to PoF light leakage decreases to sub-PE levels with these measures.

The level of detectable light leakage at the cold box was evaluated by measuring the rate of single PE signals with an independent X-ARAPUCA module mounted on the wall (V1). Data were taken while both the cathode X-ARAPUCA modules (V4 and V5) with PoF lasers were turned ON and OFF. No difference was found in the number of detected single-photon signals with PoF ON compared to PoF OFF (no laser light injected in cold box). The noise distribution evaluated from baseline fluctuations from the V1 membrane-mount X-ARAPUCA module on the wall before and after turning on PoF lasers is shown in Figure 1.33 and demonstrates no significant noise increase. It is concluded the light leakage has been reduced to inconsequential levels.

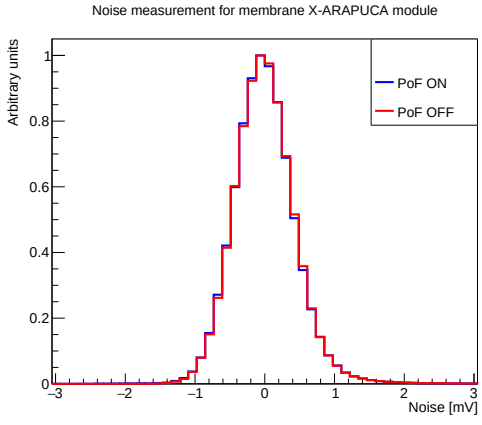

Figure 1.33: Distribution of baseline noise for membrane V1 X-ARAPUCA (DCEM v1.0 coaxial cable readout) with PoF OFF and ON for February 2023 cold box data.

Interactions between the PDS system and the rest of the detector were evaluated. The noise levels on the PDS system were compared with the cathode HV voltage ON (10 kV) and OFF. Figure 1.34 shows the Fourier transform of the data collected from a cathode module; the peak around 30 MHz corresponds to the frequency domain of the signals detected. No difference was observed due to the state of the HV. The TPC CE also evaluated the noise level with PDS on and off, finding no differences.

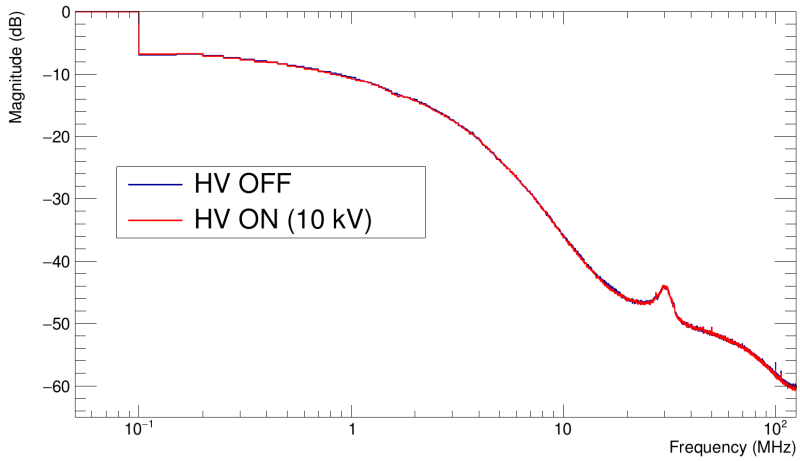

Figure 1.34: Fourier transform plot of the baseline signal of the PDS readout with the high voltage of the cathode ON and OFF. No difference is found.

Lastly, the time resolution of the PDS system is evaluated by comparing the measured time of arrival of signals from two channels for the same X-ARAPUCA; the result is shown in Figure 1.35. The convoluted time dispersion of both channels is found to be of the order of a few nanoseconds. It should be noted that the result is preliminary in that a fixed threshold is applied and with no correction for time-walk.

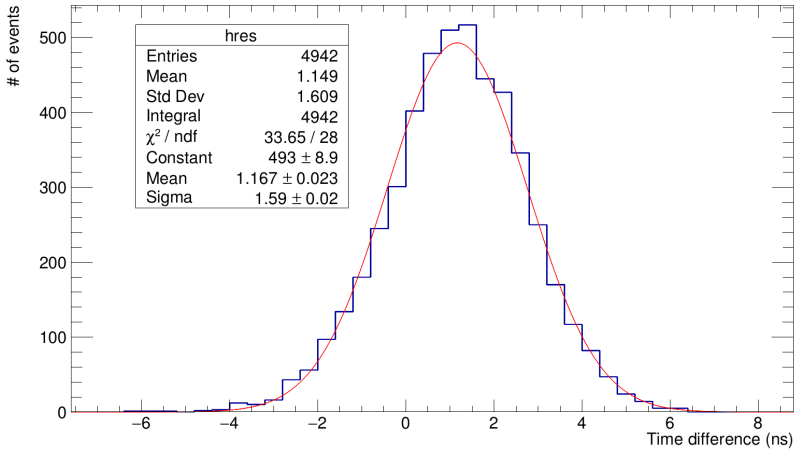

Figure 1.35: Histogram of the time difference between signals from the two channels of one X-ARAPUCA detector.

1.9 Production and Assembly

The FD2-VD PDS production phase will be launched after a successful PRR, which should be completed in early 2024.

Production procurement will be split into three phases: an initial 10% phase to establish the quality assurance (QA)/quality control (QC) procedures with vendors and FD2-VD PDS assembly centers, followed by two 45% time-sequential phases. This sequence of fabrication stages is initially envisioned to allow for an initial 10% production startup phase followed by two main production phases to control cost envelopes over fiscal years. It also provides a handle for multiple sites and/or multiple vendors, as a secondary benefit. Once production begins, the schedule drivers for FD2-VD PDS are procurement handling, vendor lead-time, and production site throughput rate. No schedule logic that interfaces to other subsystems will be present until installation begins.

The reference design calls for using several similar or identical components for FD2-VD PDS as used in FD1-HD: photosensors, dichroic filter plates, WLS plates, and membrane-mount conductive cables. Dealing with the same vendors as the FD1-HD should mitigate production delay concerns on these components. Schedule risk is significantly mitigated by a two-vendor strategy for both photosensor and WLS plate fabrication. Multiple vendors of high-quality dichroic filters have also been identified.

Planning for module assembly is based on the experience with the ProtoDUNE-SP PDS. The modules were designed to be factorizable into multiple free-standing sub-assemblies, thereby increasing the number of assembly sites that can operate independently. SiPMs already mounted to flexible PCBs will be procured from vendors, simplifying the logistics chain while reducing the number of required QC tests. Dichroic filter plates will be procured, tested and assembled into sub-assemblies as shown in Figure 1.8. These sub-assemblies will be assembled into PD modules at multiple production sites. Studies of assembly rate for FD2-VD PD modules will be conducted as part of the cold box and FD2-VD Module 0 validation efforts. Preliminary tests at CSU, NIU and at CERN all suggest that module assembly times (from a complete set of components) of one module per day using a two-person assembly team are reasonable. Particular care will be taken to understand the impact of coupling the SiPMs to the WLS plates, which is likely to have the most significant impact on production rate.

The reference plan is for 672 detector modules for the FD2-VD PDS. Potential production sites at collaborating institutions have been identified. At least two production sites will be selected, possibly more, depending on interest from collaborators and the ability to meet production requirements. These production sites will be supplied from multiple sub-assembly sites, the number of which will be determined by collaborator interest and the required production rate. It is planned to launch production orders over three years beginning in 2024 and for fabrication of core components (SiPM, WLS plates, dichroic filters etc.) with a ramp up during summer of 2024. After the ramp-up period, the target production rate for modules is eight per week. In the reference schedule, detector module assembly begins in early 2025 and should be completed by Q2 2027.

For cold electronics readout, commercial vendors will fabricate custom PCBs. On-board components will be qualified for long-term cold operation following a peer-reviewed process. PoF assembly is currently planned to involve custom assembly by collaborating institutions on the transmitter

side and for individual receiver mounting to the cold readout electronics motherboard. There is an opportunity to explore turnkey vendor assembly of the PoF rack mount transmitter units and cold receiver units. The PoF fiber optical power converter receiver unit is fabricated by commercial vendors, as is the SoF transmitter unit.

The readout electronics in warm is a custom module assembly of commercial digitizer and aggregator electronics.

1.10 Interfaces

Tables 1.9 summarizes the PDS interfaces to the other FD2-VD systems. Each interface is discussed in more detail in the following sections.

Table 1.9: PDS interface descriptions and links to full interface documents.

Interfacing System	Description
CRP	Response Monitoring System diffuser placement (potential, TBD), routing of PDS fibers at bottom of cryostat.
BDE	Shared use of cable trays and cryostat penetrations.
TDE	None.
HVS	Mechanical and electrical contact between cathode and PD modules, fiber routing in cathode, fiber routing along field cage, field cage transparency, PDS fiber diffuser placement, high voltage system (HVS) camera lighting.
DAQ	High-speed data links, timing signals.
I&I and SC	Membrane-mounted PD module support, fiber installation process, grounding, rack infrastructure, LV power, PDS readout configuration, power supply control and monitoring, PDS Response Monitoring system control and monitoring.
CALCI	None.
SWC	Software and databases to support data-taking and offline analysis.

1.10.1 Charge Readout Plane (CRP)

Previously, a potential interface between the PDS and CRP was identified as arising from the possible installation of PDS Response Monitoring System optical fibers on the central long axis of each CRP. As of the drafting of this report, it is believed that the optical fibers placed between the field cage and cryostat wall will provide sufficient coverage of all PDS modules in the system, thus eliminating this interface. This will be verified with the FD2 FD2-VD Module 0 run scheduled to take place in 2023, and the potential interface revisited accordingly.

The precise routing of bundles of fibers for the PDS PoF and SoF systems for cathode-mounted modules is a potential mechanical interface with the CRP. The interface will be further defined to ensure that the fiber bundles at the bottom of the cryostat are neither damaged by nor impede the placement of the CRP during its installation.

1.10.2 Bottom Drift Electronics (BDE)

The interfaces between BDE and PDS stem from overlapping cable and fiber paths for the two systems. As described in Section **??**, the two systems share 40 penetrations through the cryostat roof, each consisting of a four-way cross-shaped spool piece. Two vertical flanges indicated in Figure **??** serve BDE, with the top horizontal flange serving PDS. The design elements required for the routing of BDE and PDS cables and fibers through the penetrations, and the responsibilities for finalizing them, are laid out in the Interface Control Document.

The routing of cables and fibers in shared cable trays along the cryostat membrane presents another interface between PDS and BDE.

1.10.3 Cathode Plane Assembly and High Voltage System (HVS)

The mechanical and electrical contact between the cathode and FD2-VD PDS as described in Sections **??** and 1.1 presents several interfaces between the PDS and HVS. The electrical contact with the cathode will be a critical consideration due to field uniformity and the risk of cathode high voltage discharge as described in Section 1.4. The reference design envisions that each cathode module contains four PD modules with an independent set of optical fibers to provide power to each module, eliminating the risk of discharge damage resulting from transient potentials between modules. An alternative mitigation using custom-designed balun circuits as part of a conductive distribution of SiPM bias voltage between PD modules on a single cathode module is under investigation, targeting a demonstration at Module-0. Individual PD modules are further protected from the effects of discharge by a conductive mesh covering each side of the cathode openings which house PD modules and by a Faraday cage enclosing the electrical components of each cathode-mounted PD module as shown in Figure 1.11.

Mechanical supports connecting cathode-mounted PD modules to the cathode structure have been designed and deployed successfully in CERN cold box prototyping runs, and will be updated as the PDS mechanical design in finalized. Both the dry and buoyant weight of cathode-mounted PD modules must remain below their respective maxima determined by cathode flatness specifications. The cathode suspension system must be calibrated in accordance with the PD module weight; 12kg is the dry weight limit per X-ARAPUCA.

As shown in Figure 1.6, the FD2-VD PDS fiber routing from the cathode modules is expected to go along the cathode to the field cage, down along the field cage, from the anode over to the membrane wall where cathode cable routes will join PDS membrane module cable routes up to penetrations at the cryostat roof.

The process of fiber installation represents an interface with HVS in the placement of fibers along the field cage cable tray, the proximity of fiber handling, and the installation of fibers in the cathode. The fiber installation in the cathode will take place *in situ*.

The light yield specification (Table 1.1) implies a design interface with HVS through the transparency of the field cage and its impact on light collection by the membrane-mounted PD modules. All membrane-mounted PD modules are positioned within the region of 70% FC transparency.

The PDS response and monitoring system has a potential interface with the HVS through the possible mounting of light sources (diffusers and fibers) on field cage elements, respectively. This interface will be updated as the monitoring system design is finalized after the operation of FD2-VD Module 0.

A final interface with HVS is presented by infrared LEDs providing illumination for inspection cameras in HVS scope. The resulting risk of damage to powered SiPMs requires a system, to be designed, to prevent operation of SiPM bias while the camera LEDs are in use.

1.10.4 Data Acquisition (DAQ)

The FD2-VD PDS interfaces with the DAQ system through high-speed links and timing signals connected to a layer of warm readout electronics that is in FD2-VD PDS scope. The DAQ high-speed links and timing signal cables and fibers are not in FD2-VD PDS scope, nor is the supporting infrastructure such as racks, rack power, and rack monitoring. The FD2-VD PDS warm readout electronics will handle extracting timing signals and distributing them to the detector readout electronics, as well as aggregating and formatting detector data in the DAQ event structure.

1.10.5 Cryogenics Instrumentation and Slow Control (SC)

SC has several interfaces with PDS:

- SC control (configuration) and monitoring of the DAPHNE modules used for PDS readout.
- SC control (voltage level, current limits, and on/off state) and monitoring (current draw, sense voltage, on/off state) of low-voltage direct-current power supplies powering the DAPHNE crates.
- SC control and monitoring of power distribution units (PDUs) controlling distributing of AC power to PDS direct-current power supplies and PoF transmitter units.
- SC control and monitoring of the flashers for the PDS response monitoring system.

These interfaces will require implementation of software modules to reflect configuration options yet to be determined.

1.10.6 Facility, Integration and Installation Interfaces (I&I)

The PDS has an interface with Integration and Installation (I&I) in the design and execution of the installation and process. The completion of routing of fibers for PoF, SoF, and the Response Monitoring System will require coordination with other systems via I&I, as well as careful consideration for Class-4 laser safety protocols during testing of PoF functionality in place.

The reference voltage of the cold electronics for the 352 membrane-mounted PD modules will be tied to detector ground at the cryostat penetration. The reference voltage of the 320 cathode-mounted PD modules will be connected via a 1 MΩ resistor to the conductive mesh that covers each cathode cell housing a PD module.

The PDS-I&I interface also includes 40 27u racks on the cryostat roof, close to the penetrations,

housing PoF transmitter boxes and DAPHNE readout cards. An additional 4 LV power supply racks serving PDS will be located among the detector racks, approximately 25 m from the penetrations.

1.10.7 Calibration and Monitoring

While early versions of the CALCI-PDS interface document anticipated light sources potentially capable of damaging powered SiPMs and lasers capable of damaging WLS components in PDS, the scope of CALCI does not currently include such components.

1.10.8 Physics, Software and Computing

The interfaces of FD2-VD PDS with physics, software, and computing are identical in form to those for FD1-HD, impacting

- Operations
- Data products
- Database schema and management
- Software design
- Computing power.

The PDS system is expected to contribute a very small fraction of the data that is selected to be transferred to and stored at Fermilab. Data products, algorithms, and database schemas provided by SWC for FD2-VD PDS data will require different treatments of geometrical information for FD1-HD and FD2-VD. PDS will be responsible for ensuring that the technical geometry description of the FD2-VD PDS remains up-to-date.

1.11 Transport and Handling

A storage facility near the far detector (FD) site (the South Dakota Warehouse Facility (SDWF)) will be established to allow storage of materials for detector assembly until needed. Transport of assembled and tested PD modules, electronics, cabling, and monitoring hardware to the SDWF is the responsibility of the PD consortium.

Following assembly and quality management testing at FD2-VD PDS construction centers, the PD modules with associated cold readout electronics will be packaged and shipped to an intermediate cryogenic testing facility for final full-chain testing including operation in LN2 to validate detector performance. Following this, the modules will be stored in their shipping containers in the SDWF. Cables, warm readout electronics, and monitoring hardware will be shipped directly to the SDWF and stored until needed underground for integration.

Packaging plans are informed by the FD1-HD PDS experience. X-ARAPUCAs will be packaged in groups of 4 modules (matching the installation pattern), approximately $1\,\mathrm{m} \times 1\,\mathrm{m} \times 50\,\mathrm{cm}$. These shipping boxes may be gathered into larger crates to facilitate shipping. The optimal number per shipment is being considered.

Documentation and tracking of all components and PD modules will be required. Well-defined procedures are in place to ensure that all components/modules are tested and examined prior to, and after, shipping. These procedures will be presented during the FD2 PDS Final Design Review and posted in EDMS.

Information coming from testing and examinations will be stored in the DUNE hardware database. Each X-ARAPUCA will be labeled with a text and barcode label, referencing the unique ID number for the X-ARAPUCA contained, and allowing linkage to the hardware database upon unpacking prior to integration in cathode modules and membrane-mount support systems underground.

Tests have been conducted and continue to validate environmental requirements for photon detector handling and shipping. The environmental condition specifications for lighting (no exposure to sunlight), humidity (<50% RH at 70 degF), and work area cleanliness (Class 100,000 clean assembly area) apply for surface and underground transport, storage and handling, and any exposure during installation and integration underground.

Details of PD integration into the cathode and installation into the cryostat, including quality management testing equipment, tests, and documentation are included in Chapter **??**.

1.12 Quality Assurance and Quality Control

The QA and QC programs as well as the design-phase quality assurance and validation plans are based on our experience with the ProtoDUNE-SP. The FD2-VD PDS quality assurance program is focused on final specifications and drawings, and developing a formal set of fabrication procedures including a detailed set of QC procedures.

During fabrication, integration into the detector, and detector installation into the cryostat, the FD2-VD PDS QC plan will be carefully followed, including incoming materials and other inspection reports, fabrication travelers, and formal test result reports entered into the DUNE QA/QC database.

Steps in this process are detailed below.

1.12.1 Design Quality Assurance

PD design QA focused on ensuring that the detector modules meet the following goals:

- Physics goals as specified in the DUNE requirements document;
- Interfaces with other detector subsystems as specified by the subsystem interface documents; and
- Materials selection and testing to ensure non-contamination of the LAr volume.

QA for full system prototypes is underway at multiple cryogenic test sites during the design to ensure the module design achieves requirements. In particular, a series of tests is ongoing at the CERN cold box at NP02, as detailed in Section 1.8.

In addition, the lifetime of all electrical components that will be located inside the cryostat must be established. Most electronics failure mechanisms can be characterized by a (positive) activation energy and are greatly suppressed at cryogenic temperatures. One notable exception is the hot electron effect [**?**] that can limit the lifetime of NMOS transistors. For this reason, all CMOS circuits must either be designed to mitigate this damage mechanism, or be operated at reduced bias voltage. Another exception is damage to components caused by material CTE mismatch; this mechanism is especially important for capacitors [**?**].

The circuit used to read out cathode-mounted PDS units includes a CMOS operational amplifier that may be difficult to qualify for resistance to the hot electron effect. High priority will be given to qualifying this part [**?**] or finding a replacement part. A number of capacitor failures have occurred during cold box tests. High priority will also be given to establishing a procedure for selecting and qualifying capacitors.

The PDS consortium will perform design and fabrication of components in accordance with applicable requirements as specified in the relevant LBNF-DUNE QA plan. If an institution (working under the supervision of the consortium) performing the work has a previously-existing documented QA program meeting PD consortium requirements, work may be performed in accordance with their own existing program. As part of the final design review and PRR process, the reviewers will be charged to ensure that the design demonstrates compliance with the goals above.

1.12.2 Production and Assembly Quality Assurance

The PDS will undergo a QA review for all components prior to completion of the design and development phase of the project. The FD2-VD Module 0 test will represent the most significant test of near-final PD components in a near-DUNE configuration, but additional tests will also be performed. The QA plan will include, but not be limited to, the following areas:

- Materials certification (in the Fermilab materials test stand and other facilities) to ensure materials compliance with cleanliness requirements;
- Cryogenic testing of all materials to be immersed in LAr, to ensure satisfactory performance through repeated and long-term exposure to LAr. Special attention will be paid to cryogenic behavior of fused silica and plastic materials (such as filter plates and wavelength-shifters), SiPMs, cables and connectors, optical fibers and connections, and all electronics and optics operated cryogenically. Testing will be conducted both on small-scale test assemblies (including small cryostats and dewars at institutions throughout the consortium) and full-scale prototypes (including mechanical testing at the large CDDF dewar at CSU, and operational testing at CERN cold boxes, ICEBERG R&D cryostat and electronics (ICEBERG) at Fermilab, and other large cryostats available to the consortium).
- Mechanical interface testing, beginning with simple mechanical go/no-go gauge tests, followed by installation into the FD2-VD Module 0 system, and finally full-scale interface testing of the PDS into the final pre-production TPC system models; and
- Full-system readout tests of the PD readout electronics, including trigger generation and timing, including tests for electrical interference between the TPC and PD signals.

Prior to beginning construction, the PDS will undergo a final design review and PRR, where the

planned QA tests will be reviewed, and the system declared ready to move to the production phase.

1.12.3 Production and Assembly Quality Control

Prior to the start of fabrication, a manufacturing and QC plan will be developed detailing the key manufacturing, inspection, and test steps. The fabrication, inspection, and testing of the components will be performed in accordance with documented procedures. This work will be documented on travelers and applicable test or inspection reports. Records of the fabrication, inspection and testing will be maintained. When a component has been identified as being in noncompliance to the design, the nonconforming condition shall be documented, evaluated, and dispositioned as: *use-as-is* (does not meet design but can meet functionality as it is), *rework* (bring into compliance with design), *repair* (will be brought to meet functionality but will not meet design), and *scrap*. For products with a disposition of accept, as is, or repair, the nonconformance documentation shall be submitted to the design authority for approval.

All QC data (from assembly and pre- and post-installation into the cryostat) will be directly stored to the DUNE database for ready access of all QC data. Monthly summaries of key performance metrics (to be defined) will be generated and inspected to check for quality trends.

Based on the FD1-HD PDS model, we expect to conduct the following FD2-VD PDS production testing:

Prior to shipping from assembly site:

- Dimensional checks of critical components and completed assemblies to ensure satisfactory system interfaces;
- Post-assembly cryogenic checkouts of SiPM mounting flex PCBs (prior to assembly into PD modules);
- Module dimensional tolerances using go/no-go gauge set;
- Room temperature scan of complete module using motor-driven LED scanner (or UV LED array), with the final electronics in place. The readout electronics for cathode-mount PD modules will be modified to allow them to be tested at room temperature; and
- DAQ tests using DAPHNE: communication check of a test pattern generated inside DAPHNE, confirmation of SiPM bias voltage settings, and a check of the digitization of known injected charges.

Following shipping to the US reception and checkout facility but prior to storage at SDWF:

- Mechanical inspection;
- Room temperature scan (using identical scanner to initial scan); and
- Cryogenic testing of completed modules (in CSU CDDF or similar facility).

1.12.4 Installation Quality Control

PDS pre-installation testing will follow the model established for FD1-HD PDS. Prior to installation in the cathode and on the membrane walls, PD modules will undergo a room temperature scan in a scanner identical to the one at the PD module assembly facility and the results compared to results collected during fabrication. In addition, the module will undergo a complete visual inspection for defects and a set of photographs of selected critical optical surfaces taken and entered into the QC record database.

Following installation into the cathode, an immediate check for optical fiber continuity will be conducted. Spare fibers will be installed in every feedthrough, so if a bad fiber is found at this point, a spare will be used (before the cathode is raised). Following the mounting of the PD module on the membrane wall, an immediate check of cable continuity will be conducted. During this test, the PDS system will undergo a final integrated system check for expected warm response for all channels, electrical interference with other electronics, compliance with the detector grounding scheme, and power consumption.

1.13 Safety

Safety management practices will be critical for all phases of the FD2-VD PDS assembly, and testing. Planning for safety in all phases of the project, including fabrication, testing, and installation will be part of the design process. The initial safety planning for all phases will be reviewed and approved by safety experts and the DUNE safety management team in the Project Office as part of the Final Design Review and the PRRs. All component cleaning, assembly, testing, and installation procedure documentation will include a section on safety concerns relevant to that procedure and will also be reviewed during the design reviews.

Areas of particular importance to the FD2-VD PDS include:

Hazardous chemicals and cleaning compounds: All potentially hazardous chemicals used (particularly WLS chemicals such as PTP used in filter plate coating) will be documented at the consortium management level, with materials data safety sheets (MSDS) and approved handling and disposal plans in place.

Class-4 laser hazards associated with the PoF installation: Class 4 is the highest and most dangerous class of laser; by definition, a class 4 laser can burn the skin, or cause devastating and permanent eye damage as a result of direct, diffuse or indirect beam viewing. These lasers may ignite combustible materials, and thus may represent a fire risk. Class 4 lasers must be equipped with a key switch and a safety interlock. All class 4 laser operation, particularly as part of installation testing when personnel from other subsystems will be present, will be documented at the consortium management level and activities will carefully coordinated with the safety experts.

Liquid and gaseous cryogens used in module testing: Full hazard analysis plans will be in place at the consortium management level for all module or module component testing involving cryogenic hazards, and these safety plans will be reviewed in the appropriate pre-

production and production reviews.

High voltage safety: Some of the candidate SiPMs may require bias voltages above 50 VDC during warm testing (although not during cryogenic operation), which may be a regulated voltage as determined by specific laboratories and institutions. Fabrication and testing plans will demonstrate compliance with local HV safety requirements at the particular institution or laboratory where the testing or operation is performed, and this compliance will be reviewed as part of the standard review process.

UV and VUV light exposure: Some QA and QC procedures used for module testing and qualification may require use of UV and/or VUV light sources, which can be hazardous to unprotected operators. Full safety plans must be in place and reviewed by consortium management prior to beginning such testing.

Working at heights, underground: Some aspects of FD2-VD PDS module fabrication, testing and installation will require working at heights or deep underground. Personnel safety will be an important factor in the design and planning for these operations, all procedures will be reviewed prior to implementation, and all applicable safety requirements at the relevant institutions will be observed at all times.

1.14 Organization and Management

The PD consortium benefits from the contributions of many institutions and facilities in Europe and North and South America. Table 1.10 lists the member institutions.

1.14.1 Consortium Organization

Table 1.10: PDS consortium institutions.

Member Institute	Country
Federal University of ABC†	Brazil
Federal University of Alfenas Poços de Caldas	Brazil
Centro Brasileiro de Pesquisas Físicas	Brazil
Federal University of Goiás	Brazil
Brazilian Synchrotron Light Laboratory LNLS/CNPEM	Brazil
University of Campinas†	Brazil
CTI Renato Archer	Brazil
Federal Technological University of Paraná	Brazil
Instituto Tecnológico de Aeronáutica†	Brazil
University Antonio Nariño†	Colombia
Universidad del Atlantico†	Colombia
University EIA†	Colombia
Universidad Sergia Ablada	Colombia
Institute of Physics CAS	Czech Republic
Czech Technical University in Prague	Czech Republic

Laboratoire APC†	France
University of Bologna and INFN†	Italy
University of Milano and INFN†	Italy
University of Milano Bicocca and INFN†	Italy
University of Insubria and INFN	Italy
Laboratori Nazionali del Sud	Italy
University of Naples "Federico II" and INFN†	Italy
University of Ferrara and INFN†	Italy
INFN Padova	Italy
INFN Pavia†	Italy
Nikhef†	Netherlands
Universidad Nacional de Assuncion†	Paraguay
Comisión Nacional de Investigación y Desarrollo Aeroespacial†	Perú
Pontificia Universidad Catolica Perú	Perú
Universidad Nacional de Ingineria†	Perú
Chung Ang University†	South Korea
CIEMAT†	Spain
IFIC (CSIC and University of Valencia)†	Spain
University of Granada†	Spain
Edinburgh University	UK
Argonne National Laboratory†	USA
Boston University†	USA
Brookhaven National Laboratory†	USA
University of California, Santa Barbara†	USA
Colorado State University†	USA
Fermilab†	USA
University of Illinois - Urbana-Champaign†	USA
Indiana University†	USA
University of Iowa†	USA
Lawrence Berkeley National Laboratory†	USA
University of Michigan†	USA
Northern Illinois University†	USA
South Dakota School of Mines and Technology†	USA
Stony Brook University†	USA
Syracuse University	USA

The PDS consortium has an organizational structure as follows:

- A consortium lead provides overall leadership for the effort and attends meetings of the DUNE Executive and Technical Boards.
- A deputy consortium lead, who provides support to the consortium lead and has specific

responsibility for oversight of the FD2-VD PDS.

- Two technical leads, one with primary responsibility for mechanical systems, and one with primary responsibility for electronic and electrical systems. The technical leads provide technical support to the consortium lead and deputy, attend the Technical Board and other project meetings, oversee the project schedule and work breakdown structure (WBS), and oversee the operation of the project working groups.
- A Project Management Board composed by the project leads from the participating countries, the consortium leadership team and a few *ad hoc* members. The Board maintains tight communication between the countries participating in the consortium construction activity.

Below the leadership, the consortium is divided up into six working groups, each led by two or three working group conveners. Each working group is charged with one primary area of responsibility within the consortium, and the conveners report directly to the Technical Lead regarding those responsibilities. Responsible institutions have been identified for all aspects of PDS detector fabrication as indicated in Table 1.11.

The working group conveners are appointed by the PDS consortium lead and technical lead; the structure may evolve as the consortium matures and additional needs are identified.

Table 1.11: PDS deliverables and responsible institutions

Subsystem	Description	Contributing Institutions
Photosensors (SiPM)	Validation, procurement and component testing for all cathode and membrane modules.	INFN-MiB, INFN-Bo, CIEMAT, IFIC, U. Granada, U. Prague
Dichroic Filters	Validation, procurement, primary wavelength shifting thin-film deposit, and component testing for all cathode and membrane modules.	INFN-MiB, INFN-Na, CIEMAT, IFIC, U. Granada, UNICAMP, UFABC, ITA
WLS Plates	Validation, procurement, groove milling and component testing for all cathode and membrane modules.	INFN-MiB, INFN-Na
X-ARAPUCA Mechanical Frames	Procurement, fabrication, construction.	CSU, Iowa, NIU
SiPM Mounting and Ganging Cold Electronics	Validation, procurement, cold FlexBoards fabrication and testing, cold FlexBoard Integration (SiPM mounting & ganging electronics) for all cathode and membrane modules.	UCSB, INFN-MiB
Signal-Shaping Cold Electronics	Component down-select, validation, procurement, cold motherboard integration (signal conditioning stage) of all cathode and membrane modules.	FNAL, UCSB, APC-Paris, LBL, U. Mich, Iowa, NIU

SoF: Electrical-to-Optical Conversion Cold Electronics	Component down-select, procurement, cold motherboard integration (SoF stage – analog signal transmitters and driver circuitry) for cathode modules.	FNAL, UCSB, APC-Paris
SoF: Optical-to-Electrical Conversion Warm Electronics	Component down-select, procurement, warm board fabrication, construction, integration (analog signal optical-to-electrical conversion stage) for cathode modules.	APC-Paris
Signal Digitization Warm Electronics	Warm board construction (signal digitizer, DAQ interface, online software) for cathode and membrane modules.	INFN-MiB, INFN-Bo, CIEMAT, IFIC, U. Granada, SBU
PoF: Warm Transmitter and Cold Receiver	PoF Laser Module down-select, procurement, Warm Laser Box fabrication and integration, Photovoltaic power converter design, selection, procurement, cold motherboard integration (PoF stage – power optical-to-electrical conversion) for cathode modules.	FNAL, UIUC, SDSMT
PoF: Step-Up Cold Electronics	PoF Voltage StepUp Cold Electronics.	FNAL, Iowa, LBL, BNL, INFN-Mi
Cathode PDS Fibers, Cables, Flanges	Procurement, fabrication, construction, integration of all fibers, flanges, and feedthroughs for cathode modules.	FNAL, NIU, UMich, SDSMT, SBU, CAU
Membrane PDS Fibers, Cables, Flanges	Procurement, fabrication, construction, integration of all cables, flanges and feedthroughs for membrane modules.	CIEMAT, IFIC
Cathode PDS Integration in Cathode systems	Procurement of electrical (cables & balun) and mechanical cathode mounting solutions, interface mechanics, integration of cathode modules.	BNL, FNAL, CSU, NIU, Iowa
Membrane PDS Support Structure Mechanics	Procurement and fabrication of cryostat mounting solutions, interface mechanics, integration of membrane modules.	CIEMAT
Cathode PDS Response and Monitoring System	LED flashers and diffuser procurement, fabrication, integration of fibers, flanges, and feedthroughs for cathode response and monitoring system kit.	ANL, CIEMAT, SDSMT
Membrane PDS Response and Monitoring System	Procurement, fabrication, construction, integration of all fibers, flanges and feedthroughs for the response and monitoring system kits.	ANL, CIEMAT

Detector Components Qualification in Cold	Test Stands (7) construction and operation: 1. Cold electronics components 2. SiPM cold FlexBoards 3. PoF and fibers components 4. Cold motherboards signal cables	BNL, SBU, INFN-MiB, UCSB, SDSMT, FNAL, NIU, UMich
Production QA	SiPM, WLS, Dichroic Filter.	INFN-Bo, INFN-FE, INFN-MiB, INFN-Na, CIEMAT, IFIC, U. Granada, UNICAMP
X-ARAPUCA Integrated Module and Electronics Assembly	Cathode and membrane modules.	NIU, CIEMAT, U. Granada
Production QC	Test Stand construction and operation: 1. X-ARAPUCA integrated cathode Modules 2. X-ARAPUCA integrated membrane Modules	1. CSU, FNAL, NIU 2. CIEMAT, INFN-Na, INFN-Pv, INFN-MiB

1.14.2 High-Level Schedule

Table 1.12 lists key milestones in the design, validation, construction, and installation of the FD2-VD PDS. This list includes external milestones indicating linkages to the main DUNE schedule (highlighted in color in the table), as well as internal milestones such as design validation and technical reviews.

In general, the flow of the schedule commences with a 60% design review based on module performance testing at PDS consortium test stands and integration testing at the CERN cold box. Additional similar design validation follows, leading to a final design review (FDR). Following the FDR, 16 X-ARAPUCAs and required electronics, cabling, fibers, and PD monitoring system components for FD2-VD Module 0 will be built, installed, and validated at CERN. Once the data from FD2-VD Module 0 have undergone initial analysis, production readiness reviews will be conducted and module fabrication will begin.

Some parts of the FD2-VD PDS system have a long procurement cycle and will require an accelerated design review process, as shown in the milestone table. This is the case for the SiPMs, required in mid-2024 for flex PCB assembly.

A more detailed schedule for production and installation of the FD2-VD is found in Figure 1.36.

Table 1.12: Photon Detection System Milestones

Milestone	Date
Ready to begin PDS install at CERN FD2-VD Module 0	Dec 2022
PDS installation complete at CERN FD2-VD Module 0	Mar 2023
Ready for Final Design Review	**Apr 2023**
Full Detection-to-Digitization Test complete	Oct 2023
Ready for SiPMs Production Readiness Review	Jan 2024
Ready for X-ARAPUCA Production Readiness Review	Mar 2024
Ready for Warm Electronics Production Readiness Review	May 2024
Ready for Fibers, Cables, and Feedthroughs Production Readiness Review	July 2024
All Production Readiness Reviews complete	**Aug 2024**
Warm electronics units construction complete	Feb 2026
Cold electronics (Sof & PoF) construction complete	Sep 2025
Cathode and Membrane X-ARAPUCA modules construction complete	May 2027
Photon Detection System Ready for Installation	May 2027
Membrane X-ARAPUCA and Response and Monitoring system installed	Oct 2027
Cathode X-ARAPUCA installed	Feb 2028
Photon Detection System commissioned	**May 2028**
Photon Detection System project complete	**Jul 2028**

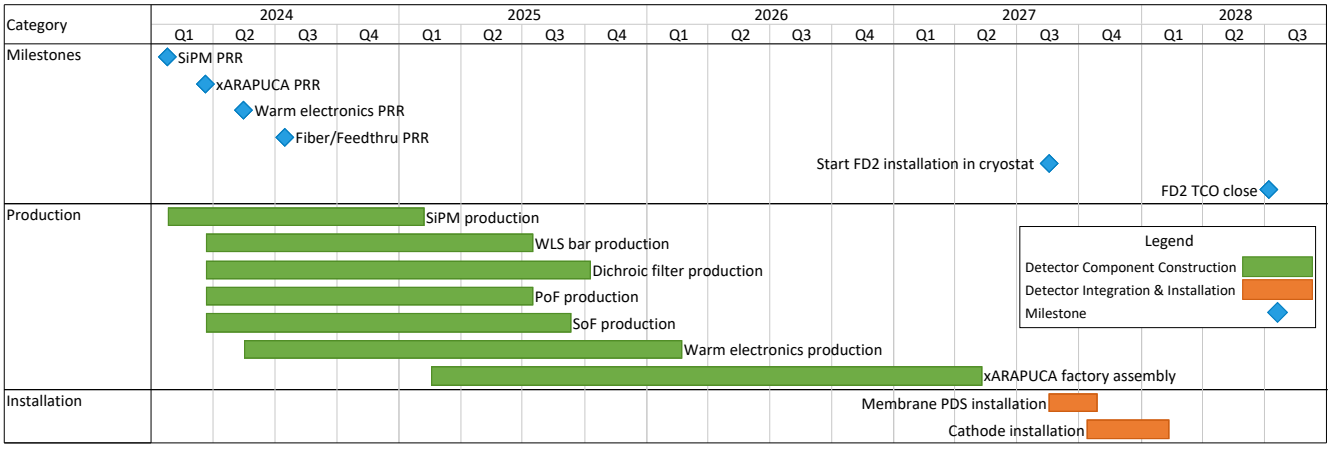

Figure 1.36: Key PDS milestones and activities toward the FD2-VD in graphical format (Data from [**?**]).